Assessing the Circulation Response to Snow Albedo Feedback in Climate Change

by

Janine Baijnath

A thesis

presented to the University of Waterloo

in fulfillment of the

thesis requirement for the degree of

Master of Science

in

Geography

Waterloo, Ontario, Canada, 2012

AUTHOR'S DECLARATION

I hereby declare that I am the sole author of this thesis. This is a true copy of the thesis, including any

required final revisions, as accepted by my examiners.

I understand that my thesis may be made electronically available to the public.

ABSTRACT

Snow Albedo Feedback (SAF) in response to climate change is a process that can amplify the climate warming response to increases in anthropogenic atmospheric CO_2 concentrations from the 20th to the 21st Century. Warmer surface air temperature may induce snowmelt and expose darker underlying surfaces which absorb more incoming solar radiation and further increase the ambient temperature. Springtime SAF in the fully Coupled Model Intercomparison Project Phase 3 (CMIP3) models is associated with summertime circulation. However, no clear physical mechanism explaining this link has been found. Furthermore, there is a large intermodel spread in the projection of SAF among the CMIP3 models which is primarily controlled through the parameterization of snow albedo in each model. Limited work was conducted on assessing the response of SAF to that of an isolated controlling parameter such as snow albedo. Here, the uncoupled Geophysical Fluid Dynamics Laboratory Atmospheric Model 2.1 (AM2.1) was used to diagnose SAF in the CMIP3 models by conducting a set of sensitivity experiments with perturbed snow albedo. This was performed to remove indirect external climate factors that may influence SAF and to use the simplified uncoupled model to understand the behaviours exhibited by the complex coupled models. Snow cover extent (SNC) and snow metamorphosis as a function of temperature (TEM) that influences SAF, as well as the knock-on effects of SAF on soil moisture, snow mass, snow melt and circulation were analyzed using both the CMIP3 and AM2.1 models. In addition, it was hypothesized that summertime Land Sea Contrast response to climate change (dLSC) is a physical mechanism that induces summertime circulation patterns in relation to springtime SAF. It is found that the AM2.1 can similarly reproduce SNC and TEM as well as the spread in SAF exhibited in the CMIP3 models. However, no robust link can be determined between SAF and its knock-on effects. Furthermore, the correlation between SAF and dLSC is not significant and thus dLSC is not a physical mechanism that influences the summertime circulation patterns in response to climate change. It is the expectation that these research results can provide an in-depth understanding of the role of SAF among fully coupled GCMs through tests performed by the uncoupled simulation.

ACKNOWLEDGEMENTS

This thesis is dedicated, in part, to all the climate change skeptics. I would not have had the courage to defend my views on this "hot" and pertinent topic if it was not for the following individuals from whom I have learned a great deal along the pursuit of my Masters Degree.

First of all, I would like to take this opportunity to thank Dr. Christopher Fletcher for giving me the most rewarding opportunity to work under his stewardship. His patience and support served as an impetus to completing this degree. Not only did he initially agree to accept me as a graduate student, but he offered me the unique experience to grow intellectually as a researcher.

I would also like to thank my committee members Dr. Claude Duguay, Dr. Ellsworth LeDrew and Dr. Richard Kelly, for readily agreeing to be an integral part of my thesis defence and for their ongoing support over the past two years. Thank you to Dr. Merrin Macre and Dr. Rich Petrone for their constructive feedback on my various assignments. I would like to also thank my various colleagues, including Adam Saunders, and the rest of my fellow group members for helping me with the various tools required for the data analyses in this research. Finally, I close by recognizing and thanking my Mom, Dad, Mike, Gran and Cho, for their unconditional love and support.

TABLE OF CONTENTS

LIST OF FIGURES

viii

LIST OF TABLES

CHAPTER 1 INTRODUCTION

1.1 Background

Increase surface warming due to anthropogenic climate change can alter the surface

albedo (α_{sfc}) over snow covered regions by changing the snow albedo of the snowpack, α_{snow}, and

the spatial extent of snow. Changes in the surface albedo induce a Snow Albedo Feedback, SAF,

which amplifies the climate warming response to increased atmospheric CO_2 concentrations.

This research examines the factors influencing SAF as well as the circulation response to SAF in

climate change. Chapter 1 commences with a background on this field of study, followed by the

literature review, motivation, objective and a brief description that outlines the structure of this

thesis.

1.1.1 Energy Budget

Earth's dynamic climate system is comprised of the coupling interactions among the

atmosphere, hydrosphere, lithosphere, biosphere, and cryosphere (Wiscombe, 2011). The

cryosphere is the second largest component of the climate after the ocean. Physical changes to

the cryosphere may induce deviations to the equilibrium climate state resulting in climate

variability or climate change. This is because of the cryosphere's high surface reflectivity, in

particular pristine ice and snow covered regions, and the latent heat associated with phase change

which has a strong impact on the energy balance (Lemke et al., 2007). Thus, the global energy

budget which depends on these components to control the gains and losses of energy within the climate system may be affected.

Approximately 70% of incoming solar radiation, insolation, is absorbed by Earth, of which, 51% is absorbed by the ground, 16% by atmospheric constituents and 3% by clouds. The remaining 30% of the total insolation is reflected away from Earth. Twenty percent of this is reflected by clouds, 6% from aerosol scattering and 4% from the ground (Ahrens, 2005). Figure 1.1shows the insolation interaction among the various atmospheric and land components. It is evident that various natural surface types will reflect and absorb a different amount of energy. This is predominantly due to the albedo of the object. Albedo has an implicit significance on influencing the global energy budget because it is a parameter that influences the ambient temperature.
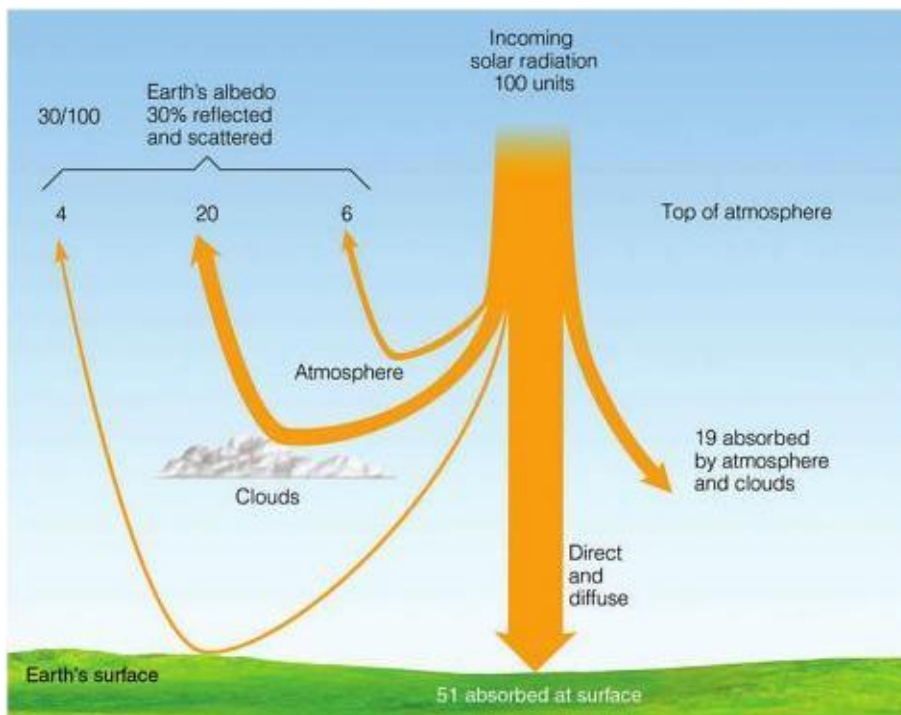
Figure 1.1: Earth's energy budget depicted as the percentage of incoming solar radiation absorbed, scattered and reflected by Earth's surface and atmosphere (Ahrens, 2005).

1.1.2 What is Albedo

Earth's radiation budget is influenced by the surface albedo (α_{sfc}). Albedo describes the optical property of matter by measuring how well it can reflect insolation. It is defined as the ratio of reflected shortwave radiation (k_{up}) to incoming shortwave radiation (k_{down}) at a particular wavelength in the electromagnetic spectrum, equation 1.1.

$$\alpha = \frac{Kup}{Kdown} \hspace{4cm} (1.1)$$

Surfaces will exhibit different albedo values depending on their physical and chemical composition. Ideal atmospheric conditions for obtaining albedo measurements are conducted during minimal cloud cover. This is because the lack of clouds limits the diffusion, mie and multiple scattering, reflection, and absorption by clouds and other atmospheric constituents on insolation.

One factor influencing albedo is the diurnal variation from the sun's angle. The angle of incidence is formed between the sunrays and the surface normal, known as the zenith angle. The size of the zenith angle will induce a weaker or higher albedo. A larger zenith angle during sunset and sunrise generates a relatively higher albedo. The albedo of water during the afternoon is between 0.03 and 0.1, whereas albedo measurements of the same water surface taken in the later evening are between 0.10 and 0.40 (Oke, 1987). The greater zenith angle allows more shortwave radiation to be reflected off the surface as the light skims the surface, compared to a smaller zenith angle which projects more direct incoming shortwave radiation towards the surface.

Other factors that influence albedo include physical and chemical properties such as colouration, texture and molecular composition. Different properties will absorb certain bands in the electromagnetic spectrum more than others. Darker surfaces absorb a large amount of insolation and only reflect a small fraction, thus resulting in a lower albedo value. For instance, densely covered vegetation canopies such as forested regimes are dominated with dark green foliage and therefore have average albedo values between 0.05-0.20 (Oke, 1987). In contrast to darker surfaces, lighter surfaces have a higher albedo because they absorb less insolation and reflect a larger amount away from the surface. Higher albedo is therefore indicative of cooler ambient environments such as in regions dominated by snow cover.

1.1.3 Snow Albedo

Relative to other natural surfaces, snow has a large albedo range. Freshly fallen snow is very pristine and white and has an albedo of approximately 0.95. However, as the physical and chemical compositions of snow change, the α_{snow} can decrease to 0.45 (Oke, 1987). Factors affecting α_{snow} are snow age, snow depth, grain size radius, the underlying α_{sfc} under a thin layers of snow, and the impurity concentrations on the snowpack, Figure 1.2 (Marshall and Warren, 1987). Over time, contaminants such as soot produced from impure carbon due to incomplete combustion of hydrocarbon, as well as cryoconite, which are windblown dust particles, accumulate and settle on the snowpack. These contaminants darken the snowpack's colour and reduce the α_{snow}. As snow melts, it accumulates a greater volume of liquid water. Since water has a lower albedo than dry snow, it will decrease the α_{snow}.

Marshall and Warren (1987) suggested that previous models assigned values of 0.55 to 0.85 for the α_{snow} of an optically thick snow depth (large snow depth). They also explain that α_{snow} usually remains constant in time until it decreases to a critical snow depth. The α_{snow} then decreases as a function of snow depth until it reaches an albedo value similar to that of the underlying surface. Figure 1.2 graphically depicts how various factors may influence α_{snow} with respect to the different wavelengths in the electromagnetic spectrum known as the spectral albedo. For the purpose of climate research the global albedo is considered where the all sky scenario is taken into consideration. By focusing on the shortwave band of the electromagnetic spectrum, this helps to differentiate the emissivity of the surface from the reflective radiation and allows the albedo to be calculated by considering the characteristics of the surface's properties. A lower albedo allows a larger amount of incoming solar radiation to be absorbed by the surface therefore increasing the surface temperature and inducing a positive feedback. The feedback of prime importance in this study is SAF which will be elaborated on in the upcoming literature review section.
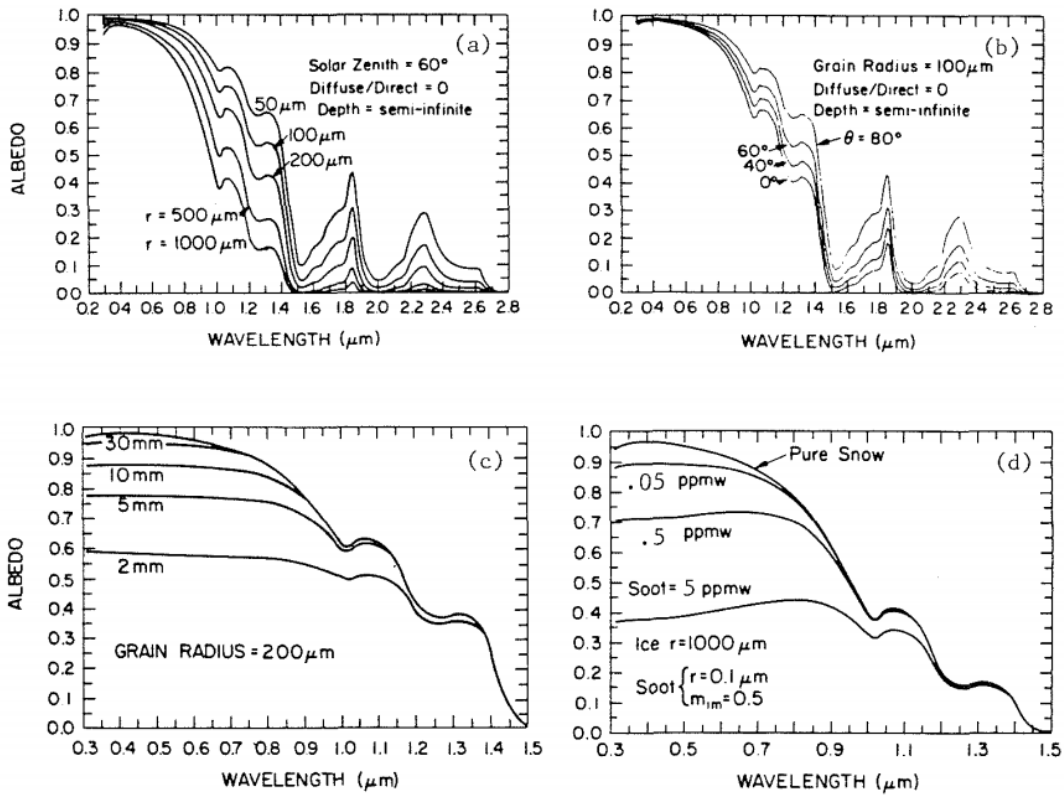
Figure 1.2: Response of surface albedo (fraction) at different wavelengths (μm) to various (a) snow granular radii (b) solar zenith angles (degrees), (c) snow depth (mm), (d) soot concentrations on snow (ppmv) (Marshall and Warren, 1987).

1.2 Literature Review

Now that the fundamentals of albedo have been established, this section presents previous work on SAF and climate change. The focus of this section is to present previous studies in this field and relate them to the current research topic. In particular the literature on SAF, fully coupled and uncoupled models, and circulation related to SAF will be discussed.

1.2.1 Snow Albedo Feedback (SAF)

SAF is a positive feedback process in the climate system that amplifies the climate warming response to an external perturbation (Bony et al., 2006). The increase of anthropogenic atmospheric CO_2 concentrations is an external forcing on the climate system that amplifies the ambient thermal energy. An initial warming to the surface may induce snow melt. This decreases the snow cover fraction on land exposing darker underlying surfaces. As a result, an increased amount of incoming solar radiation is absorbed at the surface. The increase in radiative heating further amplifies the surface temperatures and through convection, the ambient temperature also increases (Alexander et al., 2010) Figure 1.3. Cess and Potter (1988) suggested that the strength of SAF is quantified by the change in net shortwave radiation associated with the change in surface temperature in response to climate change. SAF values are affected by surface temperature, T, snow cover fraction and α_{snow}. Each climate model generates a different SAF value depending on the parameterization schemes of α_{snow} and other related variables implemented into the models.
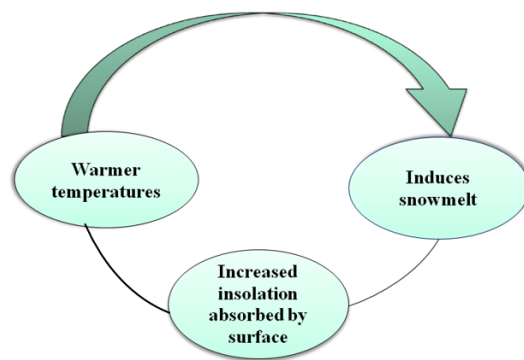
Figure 1.3: Schematic of the positive Snow Albedo Feedback process.

Research from the Intergovernmental Panel on Climate Change (IPCC AR4) shows the mean projected global surface warming response to climate change for a number of atmospheric CO_2 forcing scenarios, Figure 1.4. Each scenario shows an intermodel spread in the projected warming. One reason for this is that each model has different parameterization schemes of variables which may influence and, or induce different feedback processes. This will be explained in more detail in Chapter 2. These different parameterization schemes will yield different feedback strengths, including an intermodel spread in α_{snow} feedback, SAF, Figure 1.5. SAF results in a warming response to climate change through the decrease in α_{sfc}. Thus, it is important to investigate the role of SAF in response to climate change as it further amplifies the surface temperatures.
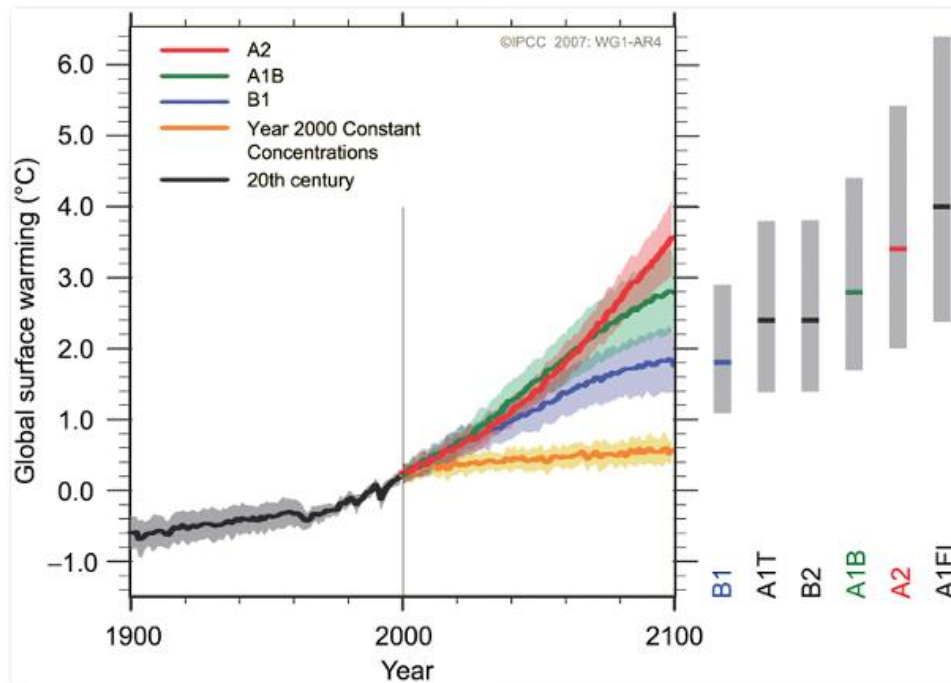
Figure 1.4: Projected global surface warming among five different CO_2 forcing scenarios ranging from high emissions (A2), medium emissions (A1B), low emissions (B1), CO_2 concentration held constant at the year 2000 (orange) and 20th Century observations (black) (Solomon, 2007).
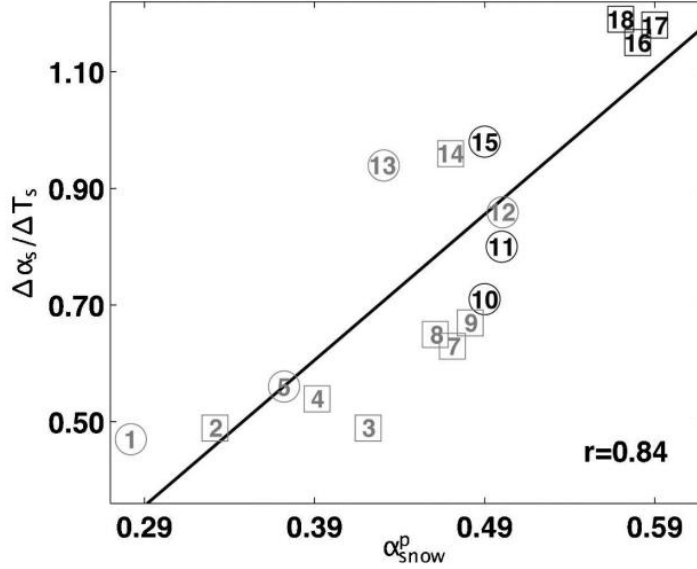
Figure 1.5: Scatter plot of SAF (%K⁻¹) with respect to present day snow albedo among 18 CMIP3 models. A least square regression line is plotted along with colour coded numbers which represent the surface albedo parameterization in snow covered areas: gray circle (Type1), gray square (Type2), black circle (Type3), black square (Type4). Refer to QH07 for details on models associated with these numbers (Qu and Hall, 2007).

Studies on SAF were conducted by a number of researchers including Qu and Hall (2007). They examined the factors influencing SAF over the 20th and 22nd Century period for land areas poleward of 30° North. More specifically Qu and Hall (2006) expressed SAF in climate change as the partial derivative of net shortwave radiation (Q_{net}) with surface temperature (T) due to changes in α_{sfc}, $\left(\frac{\partial Qnet}{\partial T}\right)_{SAF}$. SAF is the product of two terms. The first term denotes the dependence of incoming solar radiation on α_{sfc} $\left(\frac{\partial Qnet}{\partial \alpha sfc}\right)$. This partial derivative term can also be expressed as follows:

$$\frac{\partial Qnet}{\partial \alpha sfc} = -I_{TOA}\frac{\partial \alpha p}{\partial \alpha sfc} \tag{1.2}$$

where I_{TOA} is the incoming solar radiation at the Top of Atmosphere, TOA. Qu and Hall (2007) considered I_{TOA} and the ratio of planetary albedo (α_p) to α_{sfc} to be constant.

The variation in planetary albedo to the albedo of the surface represents the attenuation effect of the atmosphere on albedo. This is attributed to the fact that insolation can be absorbed by the atmosphere and radiated back to space as longwave radiation. Therefore, the amount of shortwave radiation reaching the surface could be potentially less than the initial incoming shortwave radiation. Furthermore, insolation can be backscattered from the atmosphere towards the surface, thus reducing the amount of outgoing shortwave radiation at the TOA.

Qu and Hall (2006) hypothesized that there would be a large divergence in the simulation of SAF among the General Circulation Models (GCMs) used in the IPCC AR4, with respect to this first term, $\frac{\partial \alpha p}{\partial \alpha sfc}$. This large spread may be attributed to the way the models implemented atmospheric attenuation effects due to the large differences in simulated cloud fields over land areas in the Northern Hemisphere (Qu and Hall, 2006). However the standard deviation among the models in the dependence of planetary albedo on α_{sfc} was only less than 10% of the mean. Also, models show within 10% that a given α_{sfc} anomaly results in the planetary albedo anomaly one half as large (Qu and Hall, 2007).

This method for estimating the ratio of planetary to α_{sfc} was applied to the satellite-based International Satellite Cloud Climatology Project (ISCCP) data to produce observed estimates. Most simulations in the GCMs agreed with the ISCCP to about 10%, notwithstanding the differences between the simulated and observed cloud fields. This increased the confidence in climate models because it suggested that large relative errors in the simulated cloud fields did not

produce large errors in the ratio of planetary to α_{sfc}. This suggests that another factor may be more responsible for the intermodel variability (Qu and Hall, 2006).

The second contributing term to SAF which relates exclusively to the surface process is referred to as the SAF index (Qu and Hall, 2006). It represents the sensitivity of α_{sfc} to changes in temperature and is noted that for every one degree Celsius change in T there is a change in the surface albedo.

$$\frac{\Delta\alpha}{\Delta T} = \text{SAF INDEX} \tag{1.3}$$

Combining equation (1.2) and (1.3) quantifies SAF as:

$$\left(\frac{\partial Qnet}{\partial T}\right)_{\text{SAF}} = \frac{\partial Qnet}{\partial \alpha} \frac{\Delta\alpha}{\Delta T} \tag{1.4}$$

which can also be expressed as

$$\left(\frac{\partial Qnet}{\partial T}\right)_{\text{SAF}} = -I_{\text{TOA}}\frac{\partial\alpha p}{\partial \alpha} \frac{\Delta\alpha sfc}{\Delta T} \tag{1.5}.$$

The ratio of changes in α_{sfc} to the change in surface temperature, $\frac{\Delta\alpha sfc}{\Delta T}$, over the Northern Hemisphere landmasses is thought to be the main source of the large divergence in simulated SAF among GCMs according to Qu and Hall (2006), evident in Figure 1.6. The standard deviation is about 30% of the mean, where the largest value of SAF is more than 3 times larger than the smallest value. The SAF index is therefore the predominant parameter influencing SAF because the other terms are essentially held constant in the equation. It is therefore essential to understand the factors that account for the variations in the SAF index among the models. Qu and Hall (2006) further suggested that to reduce the divergence of the SAF index among the

GCMs, attention to the parameterization of the snow process should be focused on instead of the intermodel variations in atmospheric attenuation effects on the α_{sfc}.
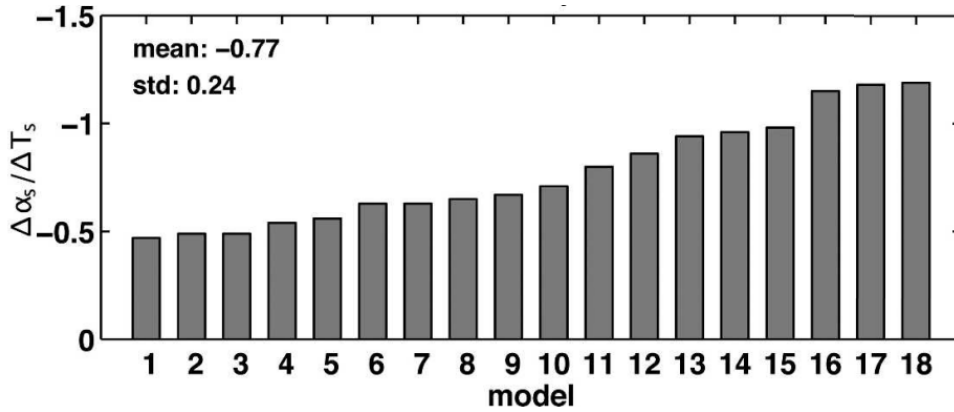
Figure 1.6: Spread in the Northern Hemisphere's extratropical, springtime SAF among 18 CMIP3 GCMs (Qu and Hall, 2007).

To validate the SAF index, here after denoted as SAF, results from previous climate models as well as observational measurements were utilized. Flanner et al. (2011) used remote sensing products from the Moderate Resolution Imaging Spectroradiometer (MODIS), as well as in-situ measurements to investigate the influence of the Northern Hemisphere's cryosphere on Earth's radiation budget at the TOA. They investigated snow cover and sea ice between the period of 1979 and 2008. They estimated that the mean Northern Hemisphere radiative forcing from TOA was between -4.6Wm^{-2} to -2.2Wm^{-2} with the maximum occurring in May of -9.0$\pm$2.7Wm^{-2}. Furthermore, they estimated a mean 30 year warming of 0.45Wm^{-2}, where the contributions from changes in snow cover on land and sea ice cover were almost the same. Flanner et al. (2011) concluded that the albedo feedback generated in the Northern Hemisphere cryosphere is between 0.3 and 1.1Wm^{-2}K^{-1}. They noted this finding to be substantially larger to

those estimates obtained in the Coupled Model Intercomparison Project Phase 3 (CMIP3) climate models.

The above findings were based on a 30 year experimental period which showed an increase in warming of about 0.79°C and 0.67°C from the GISS Surface Temperature Analysis and the Hadley Centre/Climate Research Unit (HadCRUT3v) dataset respectively. Combining these changes in surface temperature with the cryosphere radiative forcing, the mean Northern Hemisphere albedo feedback was $0.62 \text{Wm}^{-2} \text{K}^{-1}$. In the CMIP3 models between 1980 and 2010, Flanner et al. (2011), quantified the Northern Hemisphere feedback to only be $0.25 \pm 0.17 \text{ Wm}^{-2} \text{K}^{-1}$. The large difference between the climate model results and their observed estimates is perhaps due to the large spread in the different albedo feedbacks in the climate model.

They further conclude that a maximum change in α_{snow} would increase the all-sky cryosphere radiative forcing by 31%. The minimum change in α_{snow} would decrease the all-sky albedo by 15%. Work by Winton (2006) indicated that changes in α_{sfc} ($\Delta\alpha_{sfc}$) yield a larger source of variability than the partial derivative of the forcing, F, to α_{sfc}, $\frac{\partial F}{\partial \alpha sfc}$, of α_{snow} feedback within climate models. Flanner et al. (2011) explained that variability in their estimates were greater over land than for sea ice. This follows from large α_{snow} variability in snow covered regions that have heterogeneous vegetation and orography. The largest variability in $\Delta\alpha_{sfc}$ occurs over shrub lands, grasslands and sparsely vegetated terrain.

Unlike Qu and Hall (2007), who showed an intermodel spread in SAF due to the variations in α_{snow}, Levis et al. (2007) showed that much of the CMIP3 intermodel spread in SAF

is explained, not just by the α_{snow}, but by the overall albedo of the surface. However they continued to explain that the albedo in snow covered regions is still a critical factor and this was reinforced by Qu and Hall (2007) who suggested that SAF is an influential process in affecting the climate sensitivity. They were able to arrive at this conclusion based on model outputs using CMIP3 and the Community Atmosphere Model Version 3 (CAM3) coupled to a Slab Ocean Model, SOM. Levis et al. (2007) ran four sensitivity simulation experiments where the ocean temperatures were prescribed and each simulation comprised a 30 year $1xCO_2$ (355ppmv) and a 50year $2xCO_2$ (710 ppmv). Further discussions on studies using atmospheric models to investigate SAF are presented in the next section.

1.2.2 Model Simulations

Investigations into SAF using climate models were predominantly performed using coupled GCMs. However, uncoupled models have been used in a very limited body of work in investigating SAF. For example, Dutra et al., (2011) investigated the interannual snow cover variability and its influence on near surface air and soil temperatures in both a coupled and uncoupled simulation. The experiments used a 30 year climate run period where the coupled simulations were forced with climatological Sea Surface Temperature (SST) and sea ice boundary conditions. In the uncoupled simulation, the evolution of the snow dynamic properties in each time step is replaced with the climatology in the general circulation, fully coupled simulation. Three prognostic variables replaced are snow water equivalent (SWE), snow density and α_{snow}. Although Dutra et al. (2011) only investigated snow cover and snow depth, their approach to investigating the responses to these variables in a coupled versus an uncoupled

model is beneficial. This is primarily based on the premise that noise or variability in a coupled

simulation can be isolated.

Using the uncoupled model exhibits two effects. The first being that the snow cover

season, which is denoted as the settling to melting period, has the same interannual evolution as

the coupled model. The second effect is that no responses to seasonal feedbacks related to snow

cover are allowed in the uncoupled model. Dutra et al. (2011) found that snow cover area and

snow depth variability contribute to almost 60% of wintertime variability in near surface air

temperature for predominantly snow covered areas, specifically, Northern Eurasian and

American continents. Furthermore their work suggested that these regions are characterized by

stronger interannual variability in snow depth as opposed to snow cover for areas that are almost

fully covered during winter. However, interannual variability in the springtime is restricted by

the snow line regions. Their results highlighted the importance of both snow cover and snow

depth in decoupling the soil temperature from the overlying atmosphere. They suggested that

further work on snow depth should be conducted for understanding the feedback processes as

well as conducting the same experiment using an array of GCMs.

1.2.3 Circulation

Springtime SAF amplifies the summertime warming response to greenhouse gas forcing.

This response occurs predominantly over land where snow can be readily accumulated, than over

oceans. This stronger warming over land relative to that over oceans induces a thermal Land Sea

Contrast, $\frac{dT}{dx}$, here after denoted as LSC. The response of LSC to climate change, $\frac{dT}{dx}(dt)$, is

denoted as dLSC. The reason for stronger warming over land than over the oceans may be

attributed to several reasons. Fletcher et al. (2009) showed that models with stronger SAF produce a stronger surface warming response to climate change, defined as the difference between the mean of the years from 2080 to 2099 and 1980 to 1999. They showed that the projected summertime atmospheric circulation response to climate change investigated by the 17 CMIP3 models is significantly related to SAF. They concluded that on average, between 5 to 10% and a maximum between 25 to 30% of the intermodel spread in the projected circulation response to climate change is linearly related to SAF. They suggested that models with stronger SAF are associated with synoptic scale features, including low pressure systems collocated with intensifying quasi-permanent, summertime high pressure areas over the North Pacific and North Atlantic basins. They further explained that models with stronger SAF are associated with increased warming over continental interiors (Fletcher et al., 2009).

Hall et al. (2008) also showed that there is a significant correlation between springtime SAF and summertime warming over most of the United States with a correlation between 0.5 and 0.6. A potential explanation for predominant warming over land was addressed by Manabe (1987) and Wetherald (1995) who explained that springtime SAF strength and the summer climate are closely linked because SAF impacts the water storage in snow packs and soil during the winter and spring. Hall et al. (2008) explained that the models with strong winter and springtime SAF will exhibit a large reduction in snow packs and thus water storage. This water deficit that persists over the summer further reduces evapotranspiration, yielding warmer summer temperatures over land (Hall et al., 2008).

There are potentially other external factors that influence a stronger warming over land than oceans which are not directly related to SAF but, instead, to the hydrological cycle. Fasullo (2010) suggested that in response to climate change, there is a disproportionate warming over

land mainly due to the contrast in aridity. Warmer temperatures increase the amount of moisture that can be stored in the boundary layer. However, the moisture content in the atmosphere over land does not increase as rapidly as that over oceans. As a result, there is less relative humidity over the landmasses than over oceans. This is probably due to constraints on the moisture transport from the ocean associated with muted warming (Fasullo, 2010).

Furthermore Fasullo (2010) suggested that the greater warming and a weaker net greenhouse feedback result in land regions that exhibit Outgoing Longwave Radiation (OLR) that is almost twice as large as that over the oceans which contributes to a longer durational LSC. The hydrological feedback also amplifies dLSC. Also, Trenberth et al. (2005) explained that increase warming over the climate change period decreases the OLR at the top of the atmosphere which increases atmospheric temperature and moisture and this enhances the hydrological cycle. Trenberth et al. (2009) further suggested that the hydrological feedback pertaining to water vapor under the assumption of constant relative humidity approximately doubles the warming response. This is attributed to the fact that increase warming causes increased surface drying which eventually reduces soil moisture and evapotranspiration, therefore decreasing evaporative cooling and further decreasing cloud formations which amplifies surface heating even further. They suggest that the water vapor feedback is central to changes in the transport of energy especially between oceans and lands.

SAF in response to climate change, influences warming over land more than over oceans, which is further explored in Chapter 4. This is compounded by the lower heat capacity of land than ocean. On average the heat capacity of water is 4182 J kg^{-1} K^{-1}. The average heat capacity of land surfaces is typically slightly smaller than that of atmosphere, which is 1004 J kg^{-1} K^{-1} (Hartmann, 1994). The lower heat capacity of the land than ocean allows the land to have a

stronger warming response to that of oceans. This induces a stronger LSC. Previous studies have linked LSC to large scale circulation patterns. Wallace et al. (1996) explained that large scatter and variability of land temperatures between November and April reflect a strong hemispheric circulation which contributes to the Cold Ocean, Warm Land Pattern (COWL), which is generated from the temperature gradient between the ocean bodies and landmasses. Broccoli et al. (1998) also concluded that the contrast in thermal inertia between land and ocean is the main mechanism responsible for the COWL pattern. They further explained that the fluctuations in the amplitude and polarity of COWL account for a substantial fraction of the variability in hemispheric and global mean temperature on monthly timescales. Finally, Ting (1996) linked observed temperature fluctuations over the Asian and North American landmasses to the variability of the Pacific and Atlantic jet streams, and to the zonally averaged zonal flow. It is evident from the aforementioned studies cited, that there is perhaps a relation between SAF and LSC as well as springtime SAF to dLSC in the climate change context.

1.3 Motivation

The literature review section demonstrates that SAF is a good indicator of climate change because it directly responds to increased anthropogenic forcing of CO_2 emissions in the atmosphere. Also, present day snow albedo can show indications of SAF in response to climate change. Research by the IPCC AR4 presented the projected global surface warming for the 21st Century among a series of CO_2 emission scenarios, as shown in Figure 1.4. All scenarios show an increase in global surface warming up until the year 2100. Each scenario is comprised of over 17 CMIP3 GCMs. The A1B scenario is defined as not relying heavily on one particular energy

18

source but rather, it equally uses a number of improved energy supply technologies (Lemke et al., 2007). For example, by following the A1B scenario, it is evident a warming of 2.6°C. However, there is a standard deviation of +/- 0.3°C which arises from the intermodel spread in projected surface warming. This spread may be attributed to various feedback processes, including SAF. In fact, work conducted by Delworth et al. (2006) explained that two different GFDL GCMs, Climate Model 2.0 and 2.1 (CM2.0 and CM2.1) show a 2.9K and a 3.4K increase in global surface temperatures respectively. The difference in the two results is accounted for by the model's different implementations of parameters including α_{sfc} and α_{snow}, which influence SAF. Therefore, by perturbing selective parameters in the GCMs, such as α_{snow}, this will result in different SAF values. Qu and Hall (2007) explained that SAF is influenced by α_{snow}. This is evident in Figure 1.5 which shows the correlation between SAF and α_{snow} among 17 CMIP3 models.

Past studies have investigated SAF using GCMs. However, what is lacking from previous work is a designed sensitivity experiment which investigates the variables influencing SAF, along with the effects of SAF on other climate variables. Limited investigations on SAF were conducted using uncoupled models. When assessing SAF in a coupled GCM, it is difficult to isolate and perturb an independent variable such as α_{snow} in order to monitor its influence on SAF and other climate variables. This is because other climate components, including the ocean, can be prominent factors influencing the SAF response. In essence, an uncoupled investigation can be treated like a physics experiment where a sensitivity analysis is conducted. This can be performed by perturbing only the α_{snow} while holding other climate components constant. By conducting a sensitivity analysis, the uncoupled model is used as a diagnostic tool to test the components of SAF and the features associated with SAF in the CMIP3 models.

It is further evident from the literature review that SAF is associated with circulation patterns. Fletcher et al. (2009) explored springtime SAF and its association to summertime circulation patterns in response to climate change. However, since their analysis was conducted using fully coupled models, the influence of other climate components such as the ocean could have influenced their results. Furthermore, an explanation of a physical mechanism linking SAF to circulation was not provided. This research proposes that the thermal gradient between the land and ocean may be a potential mechanism linking SAF to circulation, which will be further elaborated on in Chapter 4.

Studying SAF in an uncoupled model lends to diagnosing the features associated with SAF, exhibited by the fully coupled models, in a controlled environment. This is important because uncoupled results are utilized to test whether the results generated by the fully coupled models are directly related to SAF, or whether there are other external signals influencing the results.

1.4 Objective

It is hypothesized that α_{snow} has a controlling effect on the strength of climate change (Qu and Hall, 2007). The purpose of this research is to explore the variables contributing to SAF as well as the variables influenced by SAF in response to climate change using an uncoupled model. The intent is to use the uncoupled model as a diagnostic to test whether the features associated with SAF, exhibited in a coupled model, are directly related to SAF or influenced from external components. This is done by conducting a set of sensitivity experiments by perturbing the α_{snow} in an uncoupled model from low to high to assess the components associated

with SAF. These results will be compared to those generated from the CMIP3 fully coupled GCMs to answer whether the uncoupled model can exhibit certain features including factors influencing SAF, the spread in SAF, as well as the knock-on effects, such as soil moisture, associated with SAF as seen in the fully coupled models. . The simplified uncoupled model is used to understand the behaviours exhibited by the complex coupled models. Specifically the questions that will be addressed in this research are as follows:

- Can the uncoupled model, Atmospheric Model (AM2.1) reproduce the two factors influencing SAF seen from the CMIP3models?
- Can AM2.1 reproduce the spread in SAF exhibited by the CMIP3 models?
- Can AM2.1 reproduce the knock-on effects (effects on soil moisture, snow mass and snow melt) associated with SAF, as seen in the CMIP3 models?

Furthermore this research seeks to provide a physical mechanism that links SAF to circulation. It is hypothesized that the summertime land sea contrast response to climate change (dLSC) may be a physical mechanism that induces summertime circulation patterns. To test this hypothesis the following questions will be addressed:

- Can the summertime circulation patterns associated with SAF, which were shown in Fletcher et al. (2009), be reproduced with respect to dLSC?
- Does springtime SAF have a significant influence on the summertime dLSC?
- Can the AM2.1 simulation runs reproduce the circulation patterns performed by using the fully coupled CMIP3 models?

This research, therefore, attempts to answer whether features generated from coupled GCMs, including surface warming, changes in α_{sfc}, soil moisture and circulation patterns, can be reproduced using an uncoupled model. This is performed to remove the indirect external climate factors that could influence SAF. Furthermore, by using a simplified uncoupled model this will up researchers understand the behaviours exhibited by the complex coupled models. If these results are reproducible, then perhaps further investigations using an uncoupled simulation can be an alternative approach to investigating SAF in climate change reducing computational costs and time.

1.5 Structure

This body of work comprises five chapters. Chapter 1 is the introduction and is divided into five sections. The first section provides a background on the research topic. The second presents a detailed literature review of past research conducted in this field. Here, earlier work on the investigation of SAF, coupled and uncoupled GCMs used to investigate SAF, and the circulation response to SAF are discussed. The third and forth sections provide the research's motivation and objectives respectively. The ideas presented in these sections are based on previous work conducted in this field. Finally the last section gives a brief overview of the thesis structure.

Chapter 2 presents the detailed methodological approach required for conducting these analyses. Herein an explanation on the tools used for the investigation, the numerical derivations and data processing techniques are presented. Chapter 3 and 4 test the hypotheses posed in this research. Specifically, Chapter 3 presents the results of the questions posed on SAF, that is, it investigates the variables influencing SAF along with the knock-on effects of SAF. Chapter 4

presents the results of the circulation response to SAF, while chapter 5 concludes the research by

summarizing the results. It also provides validations and limitations on the research and finally

addresses the possibility for future work on this research topic.

CHAPTER 2 METHODOLOGY

This chapter presents the approach used for producing the results discussed in Chapters 3 and 4. Chapter 3 seeks to investigate whether an uncoupled model can reproduce the intermodel spread in SAF exhibited by a number of GCMs. If it can, the question arises as to whether an uncoupled model can reproduce the knock-on effects associated with SAF. Chapter 4 seeks to compare the circulation response associated with SAF, using both GCMs and an uncoupled model. To address these issues posed in both chapters, two simulations are conducted.

The first simulation conducts investigations on SAF using fully coupled GCMs from the Coupled Model Intercomparison Project, Phase 3(CMIP3), which will be further elaborated on in the following sections. Here a detailed investigation into SAF and the factors influencing SAF are conducted using the Geophysical Fluid Dynamic Laboratory Coupled Model 2.1 (CM2.1). This GCM is designed to simulate atmospheric and oceanic climate and variability (Delworth et al., 2006). The ocean and land components are coupled allowing the models to come into equilibrium with a doubling of CO_2 (Delworth et al., 2006). This allows for the exchange of energy to occur among the oceans, land and atmosphere which in turn influence the ocean to respond to changes from these climate components.

The second simulation uses an uncoupled model, Atmospheric Model 2.1 (AM2.1) which is a subcomponent of the Coupled Model 2.1. This uncoupled model allows for the interaction between land and atmosphere. The ocean is prescribed and does not respond to energy changes in the atmosphere and land. AM2.1 is evaluated with a series of prescribed SSTs simulations (Anderson et al., 2004). This simulation is divided into three runs. Each run has a snow albedo value explicitly prescribed and is denoted by low, mid and high for the different albedo levels.

By default the snow albedo in the AM2.1 varies between 0.65 and 0.8 over all land cover types when the surface temperature is at or below the freezing point of 0°C. In order to conduct the sensitivity analysis of SAF, the snow albedo in the AM2.1 is perturbed. This was done by reducing the snow albedo for all land cover types by 0.2, to yield the snow albedo values in the mid albedo run, and by 0.4 for the low albedo run. The high albedo run remains unchanged and is the same as the initial default setting which is also the same in the CM2.1 (Fletcher, 2012).

Both simulations assess SAF and its associated variables and knock-on effects in the 20th and 21st Centuries. The simulations further investigate these responses to climate change, as the difference between the 20th and 21st Centuries. The results generated by the CM2.1 and AM2.1 simulations are compared. Also, the results generated by a series of CMIP3 models are compared to the AM2.1 runs. Firstly, a description of the tools and models required for this investigation will be provided. The data processing techniques will be explained including a number of derivations of the various variables used.

2.1 Tools and Models

This research is conducted by using numerous computer based programs. Operating on the Linux based system, experimental analyses are executed using the Climate Data Operator (CDO) and Cshell scripting. Plots are generated using the National Center for Atmospheric Research, Climate Language (NCL) and Excel. General Circulation Model (GCM) data are provided in the Network Common Data Form (NetCDF) format. The research is conducted using data exclusively from the CMIP3 GCMs. These models were also used by the International Panel on Climate Change (IPCC), Fourth Assessment Report (AR4). One of these models includes the

CM2.1which is further used in this research. Also, the AM2.1 is an uncoupled atmospheric

component of the CM2.1. It is used to conduct sensitivity analyses where the ocean component

of the climate system is prescribed. The CMIP3 models including the CM2.1 and AM2.1 are

discussed below.

2.1.1 CMIP3 Models

The outputs from seventeen CMIP3 models are used in this investigation. For the

analyses, some models are not included due to lack of available data which will be further

elaborated on in the upcoming sections. Also, in Chapter 3 the fourth generation NCAR Climate

model developed by the CMIP5 class (NCAR4) is used (Fletcher et al., 2012; Gent et al., 2011).

However, the focus will primarily be on the CMIP3 models.

The snow albedo implemented into each CMIP3 GCM is determined by considering the

effects of snow metamorphosis. The snow metamorphosis is parameterized with an explicit

dependence on temperature or snow age (Qu and Hall, 2007). The GCMs also determine surface

albedo by a specific vegetation masking type. Each model has one of four specific types. The

Type 1 scheme calculates surface albedo based on radiation transfer between the tree canopies

and the ground. The ground albedo is a weighted mean of both snow and soil albedo. In Type 2,

the surface albedo is a weighted mean of vegetation and ground albedo. The Type 3 scenario

calculates surface albedo based on snow-free land albedo and snow albedo, where the snow

albedo is dependent on the vegetation type. In Type 4, however the surface albedo is a weighted

mean between snow albedo and snow-free land albedo, with snow albedo independent of

vegetation type. Types 1, 3 and 4 have weights determined by snow cover, while in Type 2 the weights are determined by vegetation cover (Qu and Hall, 2007). Refer to Table 2.1 for a list of the models with their respective vegetation masking Type and reference.

2.1.2 Coupled Model - 2.1

CM2.1 is used to conduct various analyses into SAF. It has a spatial resolution of 2.0°latitude by 2.5° longitude (Delworth et al., 2006). The snow- free surface albedo, snow albedo and snow-masking depth are tuned on the basis of a comparison of model output with the National Aeronautics and Space Administration (NASA), Langley surface radiation budget data analyses (Darnell et al.,1988; Gupta et al.,1992; Anderson et al.,2004). The overall surface albedo implemented in this model comprises snow-free and snow albedo surfaces including snow-masking depth. The snow- masking depth is a surface parameter that qualitatively accounts for the increase in surface albedo as snow depth increases (Milly and Shmakin, 2002). CM2.1 calculates snow albedo with an explicit dependence on temperature which influences snow metamorphosis rather than snow age.

2.1.3 Atmospheric and Land Model -2.1

The CM2.1 has an atmospheric and a land component, known as the Atmospheric Model 2.1 (AM2.1) and the Land Model 2.1 (LM2.1) (Delworth et al., 2006). The AM2.1 has a horizontal grid with a resolution of 2° latitude and 2.5° longitude (Arakawa and Lamb, 1977; Anderson et al., 2004). Anderson et al. (2004) explained that the vertical coordinate encompasses a hybrid of sigma values near the surfaces and transforms to pressure values above 250hectopascal (hPa).

There are 24 vertical levels in the model. There are nine layers below 1.5km which uses a finer resolution required for boundary layer turbulence conditions. At higher altitudes of the troposphere the resolution becomes coarser at approximately 2km by 2km. There are five levels present in the stratosphere with the highest at approximately 3hPa. The fourth dimension is time which uses a two-level time differencing scheme. Gravity waves and advective terms are implemented in the model, using the forward-backward scheme and the Euler backward scheme respectively (Anderson et al., 2004). The prognostic variables in the model are zonal and meridonal wind components, surface pressure, temperature, specific humidity of water vapour, and cloud properties which will be presented next.

Radiation, clouds, surface fluxes, turbulence, and gravity waves are all parameterized in the AM2.1. Anderson et al. (2004) explained that for the prescribed radiation, the model must consider the scattering and absorption interactions between shortwave radiation and atmospheric gases such as H_2O, CO_2, O_3, and O_2. The long-wave radiation is implemented by accounting for the atmospheric gases mentioned above including emissions and absorption of N_2O, CH_4, and the halocarbon as CFC-11, CFC-12, CFC-113, and HCFC-22. Other atmospheric constituents such as aerosols and clouds are treated as absorbers to long-wave radiation. It is also noted that the model's radiation budget is tuned so that the net radiative balance is between 0 and 1Watt/m2 (Anderson et al., 2004).

Precipitation efficiency is defined as the fraction of water that is condensed to form precipitation in cumulus clouds. In AM2.1, precipitation efficiency is specified as 0.975 for deep convection which dissipates at 500hPa, and 0.5 for shallow convection which dissipates below 800hPa.The model specifies 300 particles/cm^3 over land and 100 particles/cm^3 over oceans for cloud droplet concentrations which are specified for radiation calculations. An assumption made

in the model is that clouds are overlapped. This is deemed acceptable at higher altitudes where the resolution is coarse. However, at lower altitudes where the resolution is finer, this becomes a poor assumption. The AM2.1 and LM2.1 first condense water vapour into clouds before precipitation. This, therefore, discounts some key condensation terms such as the ones associated with boundary layer condensation. A local mixing parameterization is used for layers of the atmosphere that are not part of the convective planetary boundary layer or the stratosphere. Finally, the parameterization of orographic roughness is required because of its influences in generating gravity waves and atmospheric drag. The model implements an effective roughness length that is proportional to the standard deviation of the mountainous topography (Anderson et al., 2004).

The LM2 model is the Land Dynamics model (Milly and Shmakin, 2002; Delworth et al., 2006). The model implements water storage at three distinct reservoirs which includes snowpack, plant root zones (soil water) and ground water. There are 18 distinct soil layers in which energy is stored as sensible heat. Latent heat is stored in the snow pack and in the 18 soil layers except for the top layer. It is assumed that every soil grid, excluding the top layer has 300kg/m3 of water which is susceptible to freezing. The model does not allow ground water and soil water to freeze despite below freezing temperatures. It is only when water exceeds the capacity of root zones that drainage occurs from soil water into ground water (Anderson et al., 2004). Since soil water is not allowed to freeze, there is no latent heating terms present for the subsurface. Snowmelt occurs only at the upper surface of the snowpack or at exposed glacier ice (Milly and Shmakin, 2002).

Milly and Shmakin, (2002) stated that it has become a common practice in climate

modeling to allow surface parameters to vary both globally and seasonally as a function of

vegetation and soil characteristics. In the GFDL models, the snow albedo is given as a function

of surface temperature and ranges between 0.45 and 0.6 for cells that are not glaciated. Glaciated

cells are given snow albedo values of 0.65 to 0.8 (Milly and Shmakin, 2002). Snow free surface

albedo and snow masking depth along with other land characteristics including bulk heat

capacity and thermal conductivity are treated as constants over time and are assumed to vary

among cells as a function of cell vegetation and soil type.

Milly and Shmakin, (2002) computed the AM2.1 net radiation of the energy budget as

follows:

$$R_n = R_s(1 - \alpha_{sfc}) + R_l - \sigma T^4 \qquad (2.1)$$

where R_n is the net radiation, R_s is the downward solar radiation, R_l is the atmospheric radiation,

σ is the Stefan-Boltzmann constant, and T is surface temperature. In this model, the surface

emissivity is set at unity. Surface albedo is calculated as a weighted mean of snow free albedo

(α_n), and $\alpha_{snow.}$

$$\alpha_{sfc} = (1-\beta)\alpha_n + \beta\alpha_{snow} \qquad (2.2)$$

where β = Ws/(Ws+Ws*)

where Ws is the water storage in snow-packs in mass of water per unit horizontal area and Ws*

is the snow-mask depth (R. D. Koster et al., 1996).The snow-masking depth is a surface

parameter that qualitatively accounts for the increase in surface albedo as snow depth increases. This is attributable to the fact that as land areas become more snow covered, less vegetation and surface features protrude from the snow to decrease the albedo. The derivation of variables including surface and snow albedo will be presented in the next section.

2.2 Data Processing and Variable Derivations

The CMIP3 models generate a set of raw data variables including surface temperature (T), snow cover fraction (SCF), soil moisture, snow mass and snowmelt. The AM2.1 also provides these raw data variable in addition to the outgoing and incoming shortwave radiation at the surface. The surface albedo is calculated explicitly by taking the ratio of outgoing to incoming shortwave radiation. This section will explain the data processing techniques used in converting the raw data variables into the appropriate format required for this research.

2.2.1 Temporal and Spatial Resolution

The initial data for these variables are modified into the correct format suited for this investigation. These modifications involve selecting the correct spatial and temporal resolution that includes the appropriate years, months and locations required for the investigation. The AM2.1 provides raw monthly averages over a 30 year period for each of the variables in the 20th and 21st Centuries. These periods are used because they represent the duration during which anthropogenic forcing of CO_2 is most prevalent (Solomon, 2007). At the year 2100 the atmospheric CO_2 concentration is doubled from 360ppm in 20th Century to 720ppm in 21st Century. At this time the atmospheric CO_2 forcing of 1% per year is stopped. Thus the 30 year

period along with certain seasons, including MAM or JJA are averaged over both the 20th and 21st Centuries.

The CMIP3 models, including the CM2.1 provide monthly averages for the 20th and 21st Centuries. Unlike the AM2.1 which is an equilibrium model, the CM2.1 is transient. For comparative purposes of the variables between these two models, a 20 year period in each century needs to be selected in the CM2.1. This is customary in climate research whenever a researcher seeks to represent a transient model as an equilibrium one. Therefore, the periods of 1980-1999 and 2080-2099 are selected to represent the CM2.1 in an equilibrium state. This is followed by a further selection of the months. Recall in Chapter 1 that SAF strength is most prevalent in the spring when there is an increase in insolation relative to that from the winter, and when there is still the presence of snow on the ground. Springtime SAF is therefore selected to yield the optimal SAF strength. March, April, May (MAM) will be the months averaged over for the years selected in AM2.1 and CM2.1 for the purposes conducting computations using these variables.

These variables are computed over land areas polewards of 30° North where snow surfaces are prevalent. A land masking function is performed to extract data only over land surfaces. Snow is overlaid on vegetation and soil surfaces but not surfaces that comprise ice. In fact, Greenland is removed from the analysis because it is predominantly ice covered. These computations were also conducted in previous literature including Levis et al. (2007), Hall et al. (2008), and Fletcher et al. (2009). Here, comparisons with current results and previous work can be conducted.

To compare the results generated among the models, another step is required. The 17 GCM models have differing spatial resolutions. Thus, comparing the results derived from models with different resolutions will yield biased conclusions because there is not a relative standard grid as a reference point. To negate this occurrence, the CMIP3 and AM2.1 models' native grids are interpolated onto a standardized grid with a lower resolution of 2.5° latitude by 2.5° longitude. This was done by using the maskgrid function on an arbitrary model grid, and specifying a grid size of 3600 with 144 lines of longitude and 73 lines of latitude on a Gaussian grid. This generated a resolution of 2.5° latitude by 2.5°longitude. The CMIP3 models and the AM2.1 now have a standard spatial resolution and thus, the data processing may commence to generate the required data for the research.

2.2.2 Derivation of Variables Influencing SAF

After the raw data files have been modified to the appropriate temporal and spatial resolution, they can now be used to further derive the remainder of variables. These variables include the land albedo (α_{land}), α_{snow}, snow cover contrast (SNC) which is the albedo contrast of snow-covered and snow-free land and the snow metamorphosis term as a function of temperature (TEM) (Fletcher et al., 2012). Equation 2.3 shows that the α_{sfc} depends on α_{snow}, α_{land}, and SCF since α_{sfc} is a sum of α_{snow} over snow covered areas and α_{land} for land areas without snow cover. The α_{land} is determined by masking the α_{sfc} grids with a snow cover mask that is less than 10%. Therefore the α_{land} represents grids with no snow cover, or limited snow cover less than 10%. Now that α_{land} is determined, equation 2.3 can be used to determine α_{snow}.

$\alpha_{sfc} = \alpha_{snow}.SCF + \alpha_{land} (1\text{-}SCF)$ (2.3)

$\alpha_{snow} = \{ \alpha_{sfc} - [(1\text{-}SCF) \alpha_{land}]\}/SCF$ (2.4)

Recall that α_{sfc} and α_{land} were determined by masking only land surfaces polewards of 30°N. The last variable that is needed to calculate α_{snow} is SCF. For the purpose of deriving α_{snow}, SCF is constrained to grid cells with over 10% of snow cover. This is to ensure that the α_{snow} only represents cells that are snow covered. A final check is performed to verify that the α_{land} is not greater than the α_{snow} (Fletcher et al., 2012).

Qu and Hall, (2007) developed a method to assess the contributing factors influencing surface albedo. They suggested that the relative contributions are snow cover and snow metamorphosis, which were later revised by Fletcher et al. (2012). These two factors further influence the SAF index and inevitably SAF. Figure 2.1 illustrates the relation between these two factors (Qu and Hall, 2007). The larger loop represents the snow cover feedback which is influenced by different terms, k1 and k2. Here, k1 signifies the change in SCF induced by a unit change surface temperature. This leads to term k2, which indicates a unit change in α_{sfc} by a unit change in snow cover. This infers that the increase of surface temperature will reduce snow cover and therefore reduce surface albedo.

The smaller loop represents the snowpack metamorphosis feedback which occurs concurrently with the snow cover feedback. This process is influenced by k3 which suggests that changes in surface temperature have a direct effect on the changes in the snowpack. The assumption here is that increase in surface temperature will decrease the snowpack albedo which in turn will inevitably reduce the overall surface albedo. Note that both feedback loops converge at the surface albedo term, indicating that both snow cover and snow metamorphosis influence the surface albedo. Here, k4 denotes the SAF index term, suggesting that a unit change in surface

albedo through heat exchange processes between the surface and the atmosphere, will also change the surface temperature.
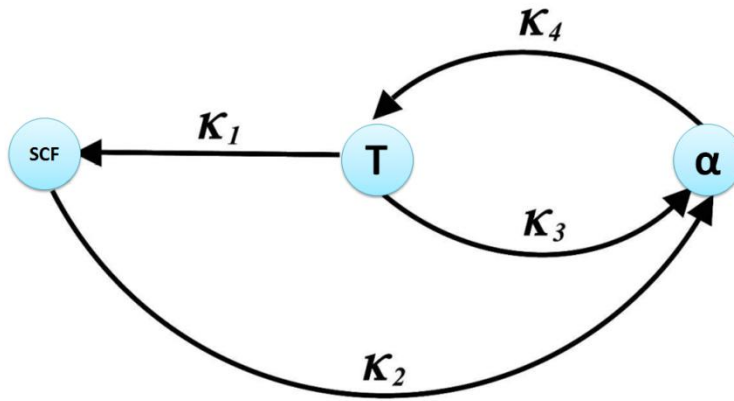
Figure 2.1: Schematic of the two feedback loops contributing to Snow Albedo Feedback. The larger loop represents snow cover contrast. Increased surface temperature leads to reduction in snow cover fraction, SCF and thus reduces surface albedo (α_{sfc}). The smaller loop represents snow metamorphosis. Increase in T reduces surface albedo of the snowpack itself. Units of k1 and k3 are $\%K^{-1}$, k2 is dimensionless and k4 is $K\%^{-1}$ (Qu and Hall, 2007).

These four k values are the constant of proportionality effects that are responsible for translating the magnitude of an anomaly in one variable to the magnitude of an anomaly in the affected variable (Qu and Hall, 2007). An initial warming (ΔT_0) arising from an external forcing sets in motion the interaction seen in Figure 2.1 where a decrease in snow cover and hence surface albedo occurs, as well as a decrease in albedo of the existing snowpack, leading finally to an additional increase in T. The incremental increase in surface temperature and surface albedo (ΔT_n) can be expressed in terms of the constants of proportionality as follows (Qu and Hall, 2007).

$$\Delta T_1 = k3k4\Delta T_0 + k1k2k4\Delta T_0 \qquad (2.5)$$

$= (k3k4 + k1k2k4)\, \Delta T_0$

$\Delta T_2 = k3k4 \Delta T_1 + k1k2k4 \Delta T_1$

The following is derived when substituting the equation of T_1 into the T_2:

$= (k3k4 + k1k2k4)^2\, \Delta T_0$

$\Delta T_n = k3k4 \Delta T_{n-1} + k1k2k4 \Delta T_{n-1}$

$= (k3k4 + k1k2k4)^n\, \Delta T_0.$ (2.6)

Assuming that k1,k2,k3 and k4 are held constant at each incremental change, the total change in surface temperature can be computed by the sum of the initial and incremental changes as follows:

$\Delta T = \Delta T_0 + \Delta T_1 + \Delta T_2 + \ldots + \Delta T_n$

$= [1 + (k3k4 + k1k2k4) + (k3k4 + k1k2k4)^2 + \ldots + (k3k4 + k1k2k4)^n] \Delta T_0$

As the series converges as n approaches infinity, ΔTs is expressed as

$\Delta T = \dfrac{\Delta T0}{1 - (k3k4 + k1k2k4)}$ (2.7)

Similarly the change in surface albedo and the change in snow cover fraction associated with each surface temperature perturbation can be derived to attain the following expressions:

$\Delta \alpha_{sfc} = \dfrac{(k3 + k1k2)\Delta T0}{1 - (k3k4 + k1k2k4}$

(2.8)

$\Delta SCF = \dfrac{k1 \Delta T0}{1 - (k3k4 + k1k2k4)}$ (2.9)

Based on the above equations we can compute the ratios:

$$\frac{\Delta\alpha}{\Delta T} = \text{k3+k1k2} \tag{2.10}$$

$$\frac{\Delta SCF}{\Delta T} = \text{k1} \tag{2.11}$$

Combining k1 equation into Equation (2.10), the expression for the SAF parameters can be expressed as:

$$k4 = \frac{\Delta\alpha}{\Delta T} = k3 + k2\frac{\Delta SCF}{\Delta T} \tag{2.12}$$

Where

$$k2 = \frac{\alpha snow(future)+\alpha snow(present)}{2} - \alpha land \tag{2.13}$$

$$k3 = \frac{SCF(future)+SCF(present)}{2}\frac{\alpha snow(future)-\alpha snow(present)}{\Delta T} \tag{2.14}$$

These equations form the two main factors that influence SAF, which are snow contrast (SNC) and snow metamorphosis based temperature (TEM). SNC is the product of k1 and k2 and TEM is denoted as k3 and are shown in Equations 2.15 and 2.16 (Fletcher et al.,2012) where the derivation of TEM and SNC were modified from that used in(Qu and Hall, 2007). The delta for SCF and T represents the change between 20th and 21st Centuries. Each century is represented as the yearly springtime, MAM average over the 20 year period of 2080- 2099 and 1980-1999 respectively.

$$\text{SNC} = (\alpha_{snow} - \alpha_{land})\,\Delta SCF\,/\Delta T_{sfc} \tag{2.15}$$

$$\text{TEM} = SCF.\Delta\,\alpha_{snow}\,/\Delta T \tag{2.16}$$

The above equations represent how the SAF, SNC and TEM terms are derived. The

variables of α_{sfc}, T and SCF are readily available in the raw data format from the models. A

programming code is written using CDO to formulate these variables in the k- coefficient form.

The k4 term is denoted as the SAF index, but again for the purpose of this study it is denoted as

SAF. The investigation computes SAF as $\frac{\Delta\alpha}{\Delta T}$ for land areas and is expressed as k4. To calculate

the snow cover component, k1 is calculated as $\frac{\Delta SCF}{\Delta T}$ and k2 is the difference between the mean

α_{snow} and α_{land}, where the mean is taken over MAM of the 20th and 21st Centuries (1980-1999 and

2080-2099). Then the product of k1 and k2 yields the SNC term. Finally, the difference between

k4 and k1k2 yields the residual term k3, which is the TEM term. It is important to reiterate that

SNC, SAF and TEM are calculated for grid cells with snow cover greater than 10% for

landmasses polewards of 30° North. SAF forms the basis of the research and is utilized in the

next section when compared to the knock-on effects.

2.3 Derivations of Variables Influenced By SAF

The knock-on effects investigated in Chapter 3 are: summertime soil moisture, springtime

snow mass and springtime snow melt. These variables are analyzed on the standard grid of 2.5

by 2.5 resolution. Land areas polewards of 30° North are again investigated with the removal of

Greenland. The soil moisture was available in raw data for all CMIP3 models excluding,

NCAR4, CSIRO, and CNRM, where no data was available. The soil moisture is constrained

between 0 and 1000kg/m^2. The values are less than or equal to 1000kg/m^2 and this is done to

remove high anomalies over certain regions in the GFDL CM2.0 and CM2.1 models, over the

regions close to the Caspian Sea. Soil moisture is bounded by the lower domain, where values

need to be greater than 0 kg/m, and where the GISS model shows negative values. Therefore, the high and low domain values are set to keep all models within a strict domain to be compared.

Snow mass was derived by a method similar to that of soil moisture. All models were used except for NCAR4 which had no data available for snow mass. The constraints of less than 1000kg or greater than or equal to 0kg are applied. The upper threshold is issued to remove anomalies from the GFDL models and the lower bound was implemented to reduce the anomalies from the GISS models, which was then applied to all models. Snow melt data is also available for all models except for NCAR4. There is no constraint assigned to the CMIP3 snowmelt data. Note that the units for snowmelt are kg $m^{-2}s^{-1}$ but is multiplied by 86400 seconds to convert units over a full day,kg $m^2.d^{-1}$. Units for soil moisture and snow mass are kg m^{-2}. The AM2.1 runs are similarly calculated, except that the monthly mean is taken over a 30 year period. Meanwhile, the CMIP3 models calculate the seasonal mean over a 20 year period. Snow mass and snow melt are measured over the springtime, MAM, and soil moisture, during summertime months of June, July August (JJA).

2.4 Procedures for Circulation Response Analyses

Chapter 4 is the second part of the results section. It investigates the circulation response to SAF and tests whether Land Sea Contrast (LSC) is a potential mechanism that contributes to the summertime circulation patterns. Chapter 4 conducts its investigation using all of the 17 CMIP3 models available along with the AM2.1 runs.

In Chapter 4 the variables LSC, T and Sea Level Pressure (SLP) are used. Initially the LSC is investigated. This is defined as the surface temperature between the land and the ocean,

$\frac{dT}{dx}$, denoted as LSC. The change in LSC, $\frac{dT}{dx}(dt)$, is here after denoted as dLSC. It is taken as

the difference between the mean of JJA summertime months, for the 20 year period in the

CMIP3 models, and 30 year period in the AM2.1 model for the 20th and 21st Centuries. The land

and ocean temperature are separately computed for areas between 30° to 60° North. The spatial

area is averaged over 30° and 60° North to ensure that when the difference is taken between the

20th and 21st centuries, the most northern grid cells are ice free. This simplifies the experiment to

ensure that the models are not taking the differences between surface temperatures that are ice

covered in the 20th Century and ice free in 21st Century (Boé et al., 2009).

Surface temperature and Sea Level Pressure (SLP) are two other variables that are

investigated in Chapter 4. These variables are computed by taking the mean over JJA for both

land and ocean surfaces polewards of 30° North. The difference, dT and dSLP, are taken as a

response to climate change. Polar stereographic maps are created with either dT or dSLP

regressed on SAF or dLSC by using NCL. The dT and dSLP files are three dimensional with

latitude and longitude dimensions that allow the variable to be spatially plotted, where a value is

assigned to each grid cell. The variables are computed by selecting the last 20 years of the 20th

and 21st Centuries, and then selecting only the months JJA. The time mean value of those three

months over the 20 year period are then determined for each century's and SLP. These yield a

time mean for T and SLP which can be spatially plotted for both the 20th and 21st Centuries. The

differences between the time means are then computed and are denoted as dT and dSLP. This is

performed for each of the CMIP3 models and placed into a file for dT and dSLP.

In regards to SAF and dLSC, these two variables are one dimensional and represent a

field mean which suggests they cannot be spatially plotted. Therefore, the same steps used in

calculating dT and dSLP are used, except after taking the time mean, the field mean is also computed. This generates only a single value of SAF and dLSC for each CMIP3 model.

NCL is then used to generate the polar stereographic regression plots. These plots represent either dT or dSLP that are regressed on either SAF or dLSC. NCL has a regression coefficient function which includes the two variables that the regression is being applied to. This then plots the regression coefficient in the polar stereographic plot. To estimate the statistical significance of the regression coefficient, the significance of the correlation coefficient is completed through using the rtest. Here it is acknowledged that the significance of the regression coefficient is not plotted, but rather the significance of the correlation coefficient is used instead. This is primarily done because plotting the significance of the correlation coefficient is a simplified alternative to compute using NCL. Also the significance of the correlation coefficient is closely related to that of the regression coefficient. Using NCL, the significance stippling is overlaid on top of the regression plots.

A regression analysis is not conducted for the AM2.1 runs because there are only three different runs over which to regress, and thus, would not yield a meaningful result. Therefore for the AM2.1 runs, the analysis is done by investigating the difference between the high and low albedo runs. The results are plots that represent dT and dSLP for which the change in the variable is in response to climate change. The variables are computed as follows. First the variables are interpolated onto the same grid as that used by the CMIP3 standard grid. The mean surface temperature and the mean sea level pressure are computed for JJA over the 30 year period. This is separately computed for the high and low albedo runs in each century. Next, the difference between the high and low albedo runs is computed for both centuries. Figures 4.5 (a) and (c) in Chapter 4 show this for the 20th Century. The difference between these values is then

taken between the 20th and 21st Centuries to assess the variables response to climate change. The results generated from these methods, will be discussed in the following chapters.

MODEL	SNOW ALBEDO	VEG TYPE	REFERENCE
MRI CGCM2.3.2	TEMPERATURE	TYPE 1	Yukimoto et al. (2006)
CGCM3.1 (T47)	SNOW AGE	TYPE 2	Verseghy et al. (1993)
CGCM3.1 (T63)	SNOW AGE	TYPE 2	Verseghy et al. (1993)
IAP FGOALS	SNOW AGE	TYPE 1	Yu et al. (2004)
MIROC3.2	SNOW AGE	TYPE 1	Takata et al. (2003)
UKMO HADCM3	TEMPERATURE	TYPE 3	Cox et al. (1999)
MPI ECHAM5	TEMPERATURE	TYPE 2	Roeckner et al. (2003)
UKMO HADGEM1	TEMPERATURE	TYPE 3	Essery et al. (2001)
IPSL CM4	SNOW AGE	TYPE 3	Chalita and Le Treut (1994)
MIUB_ECHO_G	TEMPERATURE	TYPE 2	Roeckner et al. (1996)
INM_CM3.0	TEMPERATURE	TYPE 4	Alekseev et al. (1998)
GFDL CM2.0	TEMPERATURE	TYPE 4	Milly and Shmakin (2002)
GFDL CM2.1	TEMPERATURE	TYPE 4	Milly and Shmakin (2002)
CNRM_CM3	SNOW AGE	TYPE 2	Douville et al. (1995)
GISS_ER	SNOW AGE	TYPE 2	Hansen et al. (1983)
CSIRO MK3_0	SNOW AGE	TYPE 2	Gordon et al. (2002)
NCAR 3 CCSM3_0	SNOW AGE	TYPE 1	Gent et al., 2011

Table 2.1: List of the CMIP3 General Circulation Models used in this research including a description of surface albedo parameterizations and references (Qu and Hall, 2007).

CHAPTER 3 SNOW ALBEDO FEEDBACK

In this chapter, a sensitivity analysis is conducted by perturbing snow albedo in an uncoupled model from low to high to assess whether the components associated with SAF can be successfully reproduced from that of GCMs. It is hypothesized that snow albedo has a controlling effect on climate change and thus the three different snow albedo runs investigated will yield different climate responses.

To test this hypothesis, investigations into the variables that influence SAF are first explored. These variables include land temperatures, surface albedo, snow cover, snow albedo and land albedo. They are tested under the low, mid and high albedo runs in climate change, using the uncoupled Atmospheric Model 2.1 (AM2.1). The different albedo runs, here after referred to as the runs. These variables are then compared to those generated from the Coupled Model 2.1 (CM2.1) to determine whether the uncoupled experiments yield similar results to those conducted by using a fully coupled GCM.

Secondly, similar comparisons will be made on two influential factors on SAF. The two factors that will be investigated are Snow Contrast (SNC) and changes to snow metamorphosis primarily due to changes in temperature (TEM). If it is identified that these components can be replicated by the AM2.1 runs, then the research will assess whether the spread in SAF among the CMIP3 models can be replicated by the AM2.1 simulations. If this spread can be reproduced in the AM2.1 then the question arises as to whether the AM2.1 runs can further replicate the knock -on effects produced in the fully coupled GCMs. The knock-on effects that will be explored include summertime soil moisture and springtime snow mass and snowmelt.

3.1 Variables Contributing to SAF in Response to Climate Change

The variables that influence SAF are investigated in this section. The variables include surface temperature, surface albedo, snow cover fraction, land albedo, and snow albedo, which are computed over the springtime, climate change period (21st Century – 20th Century) for the Northern Hemisphere, poleward of 30° North. Recall from Chapter 1, Equation (1.5), that SAF is the product of two terms. The first term represents the ratio of the planetary albedo to surface albedo, multiplied by insolation at TOA. There is a small intermodel spread in this term and most models agree within less than 10% of the ensemble mean (Qu and Hall, 2006). As mentioned in Chapter 1, since this term is not the main contributor to the CMIP3 intermodel spread in the total SAF strength, then the attention is turned to the second term, which is the SAF index. Recall that for the purpose of this research, the SAF index is denoted as just SAF, which is the ratio of the change in surface albedo to change in surface temperature, $\frac{\Delta\alpha}{\Delta T}$. SAF diverges widely among the models and is therefore worth investigating in more detail (Qu and Hall, 2006).

SAF is a function of the change in land surface temperature (ΔTland). This is defined as the change in land surface temperature in response to climate change, where climate change is denoted as the mean of 2080 to 2099, minus the mean of 1980 to 1999. The ΔTland is averaged over springtime, March, April May (MAM) and is computed for the AM2.1 runs and CM2.1. In both the CM2.1 and AM2.1 simulations, it is evident, from Table 3.1 that the land surface temperature in each century (Tland) increases from the 20th Century to 21st Century, as a result of increase atmospheric CO_2 concentrations. In comparing the AM2.1 runs, it is established that the Tland decreases in the 20th and 21st Centuries for the higher albedo run, compared to that of the low run. This indicates that models with higher surface albedo will yield colder Tland and this is

readily demonstrated if the α_{sfc} is higher. This in turn will reflect greater incoming solar radiation higher back to the atmosphere and outer space.

VARIABLES	LOW			MID			HIGH			CM2.1		
	20C	21C	Δ	20C	21C	Δ	20C	21C	Δ	20C	21C	Δ
Tland (K)	277.6	280.0	2.5	276.9	279.5	2.5	275.5	278.5	3.1	272.6	276.5	3.88
α_{sfc}	0.228	0.175	-0.057	0.263	0.206	-0.061	0.330	0.251	-0.080	0.367	0.282	-0.091
SCF	0.21	0.20	-0.01	0.25	0.23	-0.02	0.31	0.28	-0.04	0.35	0.30	-0.05
α_{snow}	0.24	0.25	0.01	0.36	0.37	0.01	0.50	0.52	0.02	0.54	0.53	-0.01
α_{land}	0.14	0.14	0.0	0.14	0.14	0.0	0.14	0.14	0.0	0.15	0.15	0.0

Table 3.1: Climate variables response to AM2.1 low, middle and high albedo runs as well as the CM2.1 simulation, for the 20th, 21st and climate change response (difference between 20th and 21st Centuries). Land surface temperature (K), surface albedo and snow cover fraction are averaged polewards of 30°North for all grid cells. Snow albedo is averaged polewards of 30°North for grid cells greater than 10% snow cover. Land albedo is the difference between surface and snow albedo. AM2.1 simulations are averaged for a 30 year period for each century. CM2.1 is averaged over the last 20 years for both the 20th and 21st Centuries.

Comparing Tland between the AM2.1 and CM2.1 simulation, it is apparent that Tland is warmer in all of the AM2.1 runs in the 20th Century and 21st Century than in the CM2.1. Figures 3.1(a) and (b) present the 20th Century, MAM Tland for the CM2.1 and AM2.1 simulations respectively. They spatially show that the cold airmass is larger for the CM2.1 simulation than the AM2.1 high run. Tland in the AM2.1 simulation is warmer polewards of 30°N than in the CM2.1. In particular the CM2.1shows colder temperatures extending all the way down to the Hudson Bay Lowlands in North America as well as colder temperatures in Sourthern Russia.

The AM2.1 tends to keep the colder temperatures straddled up towards the Northwest territories as well as further Northeast over Eurasia.

Potential reasons for the colder Tland exhibited in the CM2.1 may be attributed to the following: CM2.1 has a colder bias primarily due to the variations in the oceans parameterization (Anderson et al., 2004). This is further reaffirmed by the fact that the CMIP3 models generally have a slight, but colder bias relative to observations (Solomon, 2007). There is a large intermodel spread in errors found in the North Atlantic Ocean. This is because the models have difficulites locating the North Atlantic currents, which are regions of warmer SSTs. These difficulties in locating the North Atlantic curents may be responsible for generating a cold bias among the models. This is mostly evident in the Northern Hemisphere middle latitutes where zonally averaged SSTs are found to be too cold (Solomon, 2007).

It is also noted that the AM2.1 simulation suppresses evaporation from land when the ground is frozen at depths of 30cm.The reduction in evaporation decreases cloudiness at higher latitudes in the Northern Hemisphere during the late spring and early summer (Delworth et al., 2006). This increases the incoming shortwave radiation hitting the surface, enhances surface temperatures and also contributes to the thinning of Arctic sea ice. This could further suggest why the AM2.1 simulation has a warmer Tland than the CM2.1.

These may be potential reasons why Tland is warmer in the AM2.1 simulation. This is further reinforced by the results of the annual Tland and SST in the CM2.1 and AM2.1 high albedo run, Figures 3.2(a) and (b) respectively. The North Pacific and Atlantic Oceans show warmer surface temperatures over a wider area than that seen in the CM2.1 simulation.
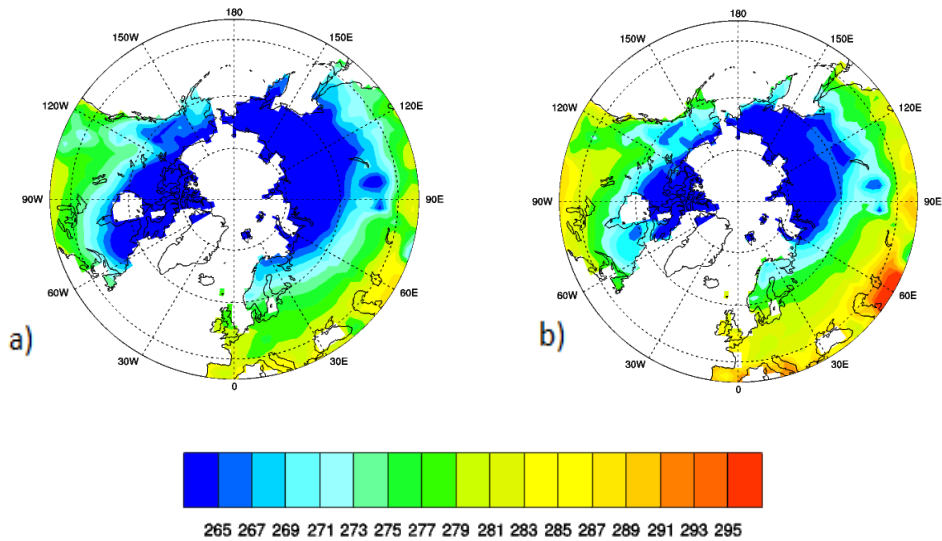
Figure 3.1: Mean MAM land surface temperature (Kelvin) for 20th Century polewards of 30°North for (a) CM2.1 between 1980 and 1999, 20 year mean, (b) AM2.1, 30 year mean.
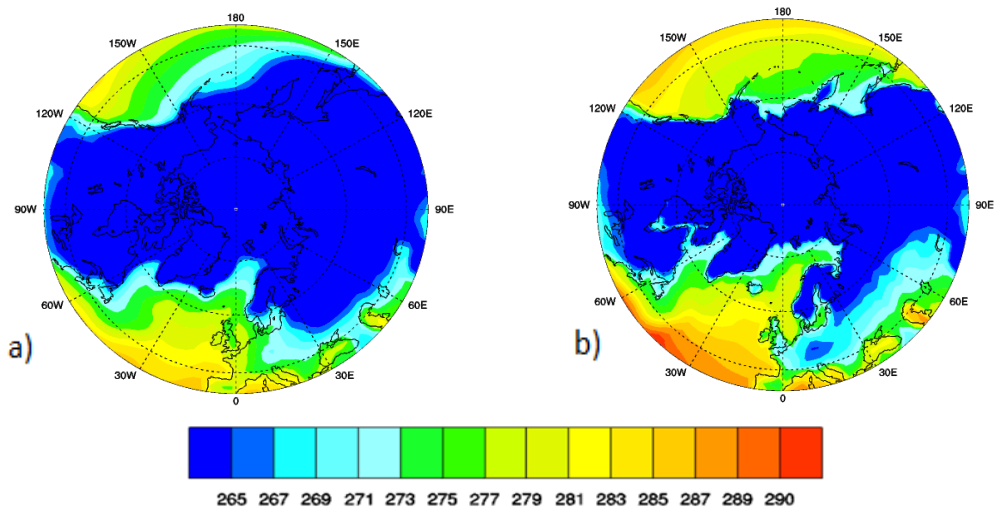
Figure 3.2: Annual mean surface temperature (Kelvin) for 20th Century polewards of 30°North for (a) CM2.1 between 1980 and 1999, 20 year mean, (b) AM2.1, 30 year mean.

Table 3.1 shows that in all simulations and runs, Tland increases from the 20th to the 21st Century. This indicates that temperatures have warmed in response to climate change. This is not surprising as the results are generated from the model which adopts the SRESA1B scenario which is characterized by having a balanced emphasis on all energy resources. This reiterates that anthropogenic emission of atmospheric CO_2 is still an influential factor inducing surface temperature warming (Solomon, 2007).

The ΔTland in the AM2.1 high run has the largest value at 3.1K compared to the mid and low runs. However, ΔTland in the CM2.1 simulation is greater at 3.9K. Recall that Levis et al. (2007) showed that models with higher snow albedo will exhibit a greater ΔTland in response to climate change. Levis et al. (2007) attributed this result to the fact that models with higher snow albedo are colder due to a greater snow mass to melt. This greater prevalence of snow will induce stronger SAF and further amplify surface warming, thus, increasing ΔTland.

Figure 1(c) from Levis et al. (2007) is reproduced herein Figure 3.3 using the present research methods. Overlain on this figure are the AM2.1 runs. This shows the relationship between ΔTland and the 20th Century snow albedo for both simulations. It is evident that both the AM2 scenario and the CMIP3 runs show a similar positive correlation between the change in surface temperature and snow albedo. However, although the different surface albedo generates a clear difference in ΔTland, the AM2.1 does not accurately represent the distribution from the CMIP3 models. The differences in ΔTland among the different AM2.1 runs are not significantly different and thus do not well reproduce the distribution pattern seen in the CMIP3 models.

Further, Figure 3.4(a) shows that a very prevalent ΔTland occurs over Northern Canada and dips as far south to the Great Lakes. There is a further increase in warming over the Eurasian

inland and although the similar spatial strengths of ΔTland are apparent, the AM2.1 simulation, seen in Figure 3.2(b) is not as strong as those seen in the CM2.1 in Figure 3.4(a). It can be concluded that the increase in warming from the 20th to the 21st Century is apparent among the AM2.1 runs as well as the CM2.1 simulation. However the CM2.1 simulation shows a greater ΔTland than the high AM2.1 run.
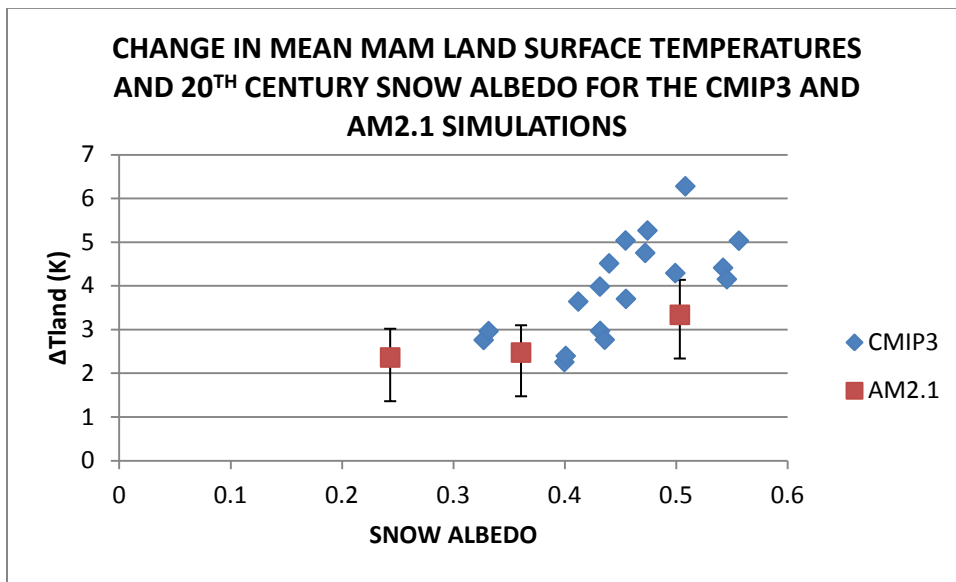
Figure 3.3: Change in mean MAM land surface temperature between the 20th and 21st Centuries, polewards of 30° North plotted against 20th Century MAM snow albedo averaged polewards of 30° North for grid cells greater than 10% snow cover, for the CMIP3 models (blue) and AM2.1runs (red) (Levis et al., 2007).
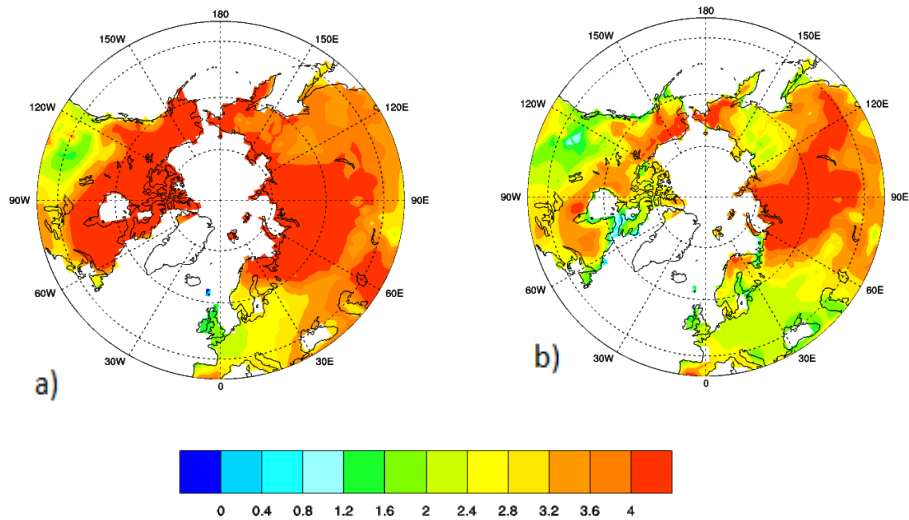
Figure 3.4: Change in mean MAM land surface temperature (Kelvin) polewards of 30°North for (a) CM2.1 (b) high AM2.1 run.

Apart from the surface temperature, SAF is also a function of the change in surface albedo in response to climate change ($\Delta\alpha_{sfc}$). Surface albedo decreases from the 20th to the 21st Century in both the CM2.1 and the AM2.1 simulations. The change in surface albedo among the AM2.1 scenarios indicates that the high albedo climate is indicative of a larger $\Delta\alpha_{sfc}$. According to the previously mentioned analysis of ΔTland, it is evident that models with a higher albedo will exhibit larger ΔTland. As a result, it is expected that this amplified warming would also influence surface albedo, which is attributed to the SAF process.

Surface albedo is dependent on the sum of two products; the first product being of α_{snow} and SCF, and the second being of α_{land} and one minus the snow cover fraction, refer to Equation (2.3). There is not a large $\Delta\alpha_{snow}$ generated within each AM2.1 albedo run. The standard deviation for the AM2.1 low and mid 20th and 21st Centuries α_{snow} is +/- 0.03, and for the high

run is +/-0.05 which indicates the α_{snow} for the 20th Century is not signficantly different from that of the 21st Century. However, it is evident that the 20th and 21st Centuries α_{snow} values increase among the AM2.1 runs. This is because they were explicitly perturbed for the purpose of this sensitivity experiment. Interestingly, $\Delta\alpha_{snow}$ is larger for the AM2.1 high run than the mid and low runs. This could be due to the fact that models with higher α_{snow} exhibit greater ΔTland which may further decrease the α_{snow}.

The α_{land} variable remains constant for each scenario as well as for each century. In the AM2.1 simulation it is not expected that vegetation type and canopy cover will be altered due to changes in agriculture and urbanized development. Therefore it is not expected that the α_{land} will change dramatically in response to climate change, and among the three AM2.1 runs. However, the one variable that does drasticaly influence the surface albedo in the different AM2.1 run is SCF. This variable decreases in response to climate change among all simulations and AM2.1 runs, primarily due to increase in surface temperatures.

Results among the variables in the AM2.1 albedo runs exhibit similar responses to those accepted by the scientific community. That is, surface temperature increases in response to climate change as a result of increasing atmospheric CO_2. However, the ΔTland is the largest for the high run which indicates that models with higher albedo exhibit a larger ΔTland (Levis et al.,2007). It is also expected that α_{sfc} is larger for the AM2.1 high run because models with higher albedo are associated with colder temperatures, and larger snow fraction. The α_{snow} is also higher for the AM2.1 high run. This may be attributed to the fact that models with colder temperatures exhibit fresher, pristine snow fall and less snow metamorphism (Marshall and Warren, 1987).

3.2 The Two Components Contributing to SAF

The previous section investigated the fundamental variables associated with SAF. Using these variables, two influential components affecting SAF are derived, recall Equations (2.5) and (2.6). The question now arises as to whether the AM2.1 simulation runs can reproduce the spread of these two factors in the CMIP3 models shown in Qu and Hall, 2007 and Fletcher et al., 2012.

The two factors that contribute to SAF are snow cover contrast (SNC) and snow metamorphosis as a function of temperature (TEM) (Qu and Hall, 2007; Fletcher et al., 2012). These two factors are a decomposition of the total SAF which is related to the temperature dependence of snow albedo (Fletcher et al., 2012). Snow metamorphosis, predominatly influenced by soot depositand internal temperature change of the snowpack decreases the α_{snow}. Increase in warming can induce snowmelt which alters the crystalline structure of the snow grains and reduces the α_{snow}. The TEM term represents the change in snow albedo over the change in surface temperature over a fixed snow covered region and thus, any changes observed in the surface albedo are primarliy due solely to TEM (Fletcher et al., 2012).The SNC component is denoted as the albedo contrast between snow covered regions and snow free regions (Fletcher et al., 2012). This SNC component is derived from the snow cover fraction, which is sensitive to changes in surface temperature.

The TEM and SNC components are computed for both the CMIP3 models and the AM2.1 scenarios. This is conducted to establish whether the relative contributions of SNC and TEM patterns can be reproduced in the AM2.1 runs. Figure 3.5 shows the relationship between TEM and SNC for the CMIP3 models in descending order of SAF strength. Models with a

higher SAF exhibit a larger SNC value. A similar distribution pattern can be seen among the AM2.1 runs, Figure 3.6.

In the AM2.1 high run, the SNC term is approximately 32 times larger than that of TEM, and in the CM2.1 simulation, SNC is approximately 5 times larger, Table 3.2. This indicates that the change in surface albedo, that influences SAF, is primarily due to the changes in snow cover contrast rather than the changes in the snow albedo of the snowpack and thus agrees with the same findings from Qu and Hall, (2007). Furthermore, remotely sensed APP-x satellite observations also conclude that SNC contributes to 69% of SAF while TEM contributed to 31% (Fletcher et al., 2012).

TEM in the CM2.1 is about 6 times higher than TEM in the AM2.1 high run. It is not clear as to why this is the case. It is speculated that this is due to the minimal $\Delta\alpha_{snow}$ in the AM2.1 runs, refer to Table 3.1. It is also speculated that the lower AM2.1 TEM values can be due to the fact that the overall AM2.1 surface temperature is warmer than that of the CM2.1, recall Figure 3.2. This is because colder environments tend to be influenced more by TEM than warmer regions. In observations, SNC dominates the total SAF at latitudes equatorward of 65°N while TEM dominates over the Arctic, peaking in localized coastal regions (Fletcher et al., 2012). Fletcher et al. (2012) suggested that colder regions retain snow for a longer duration of time which therefore undergoes snow metamorphosis. Considering this, it is therefore suggested that models with warmer climates will exhibit lower TEM values. This is a suggested area for which further investigations may be required.
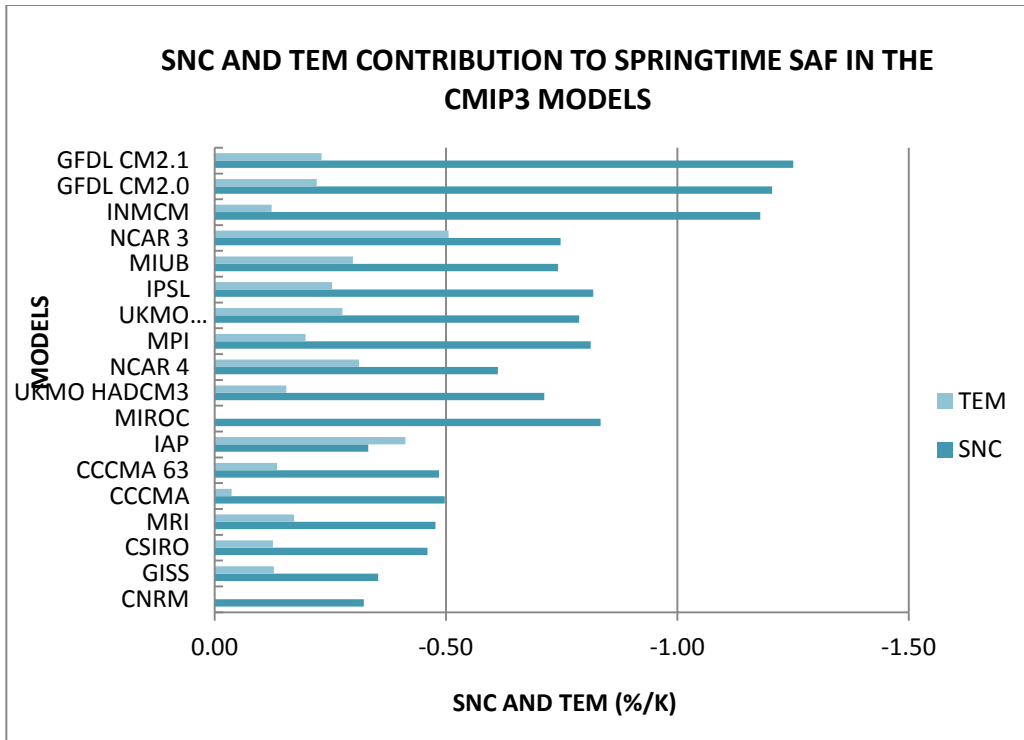
Figure 3.5: Snow cover contrast (dark blue) and TEM (light blue), units in %K^{-1}, for the CMIP3 models arranged from strongest (top) to weakest springtime SAF.
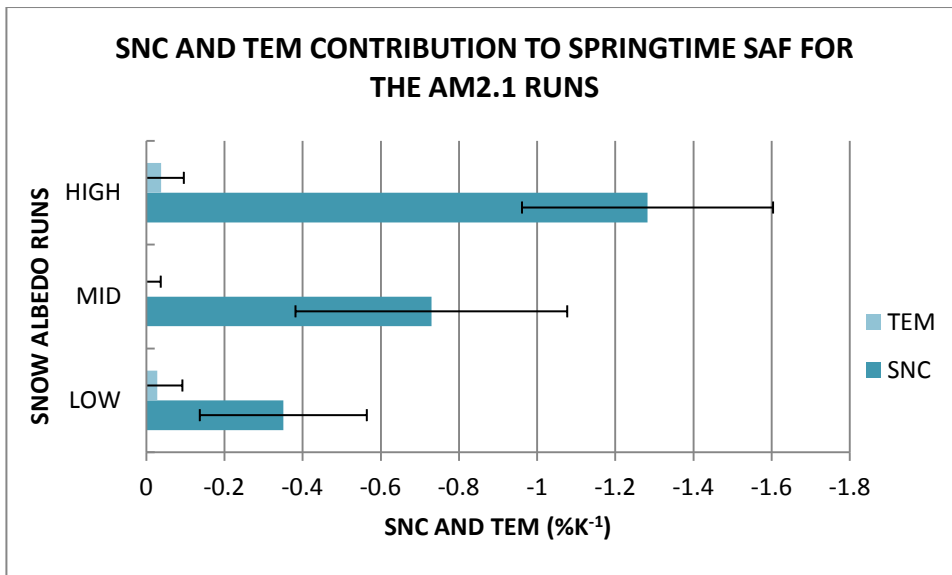
Figure 3.6: Snow cover contrast (dark blue) and TEM (light blue), units in %K^{-1}, for the AM2.1 simulation runs arranged from highest (top) to weakest snow albedo runs.

VARIABLES	LOW	MID	HIGH	CM2.1
SNC	-0.36	-0.73	-1.28	-1.25
TEM	-0.03	0.02	0.04	-0.23

Table 3.2: SNC and TEM (%K^{-1}) for the three albedo runs in the AM2.1 simulation and the CM2.1 simulation.
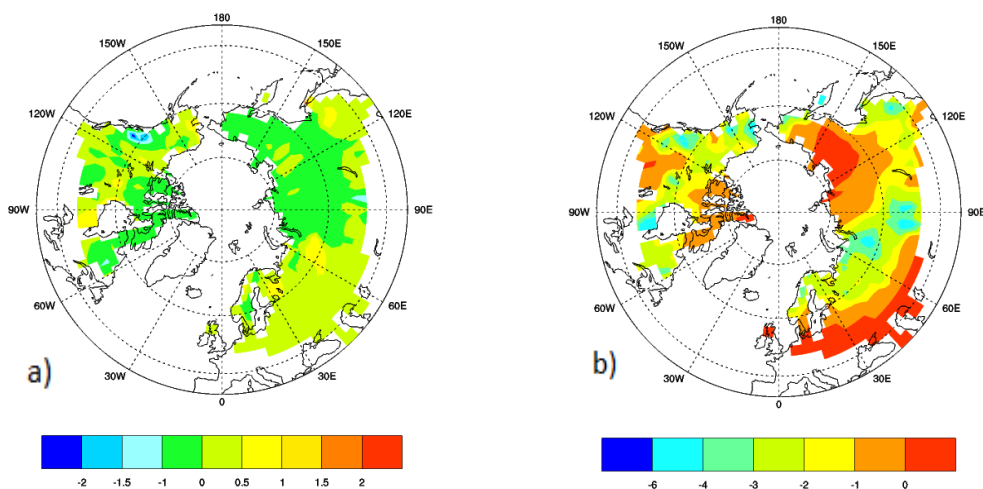
Figure 3.7: AM2.1 high albedo run for land areas polewards of 30° North for (a) TEM(%K^{-1}), (b) snow cover contrast SNC (%K^{-1}).

3.3 Reproducing the Intermodel Spread in SAF

Since the factors influencing SAF can be reproduced by the AM2.1 run, the focus is now turned to establishing whether the spread in SAF among the CMIP3 models can be replicated in the AM2.1 simulation. Qu and Hall, (2007) showed that the spread in SAF exhibited by the CMIP3 models is primarily due to the model's snow albedo. Figure 3.8 shows the relationship between SAF and effective snow albedo which yields a positive correlation with an r value of

0.8. Overlaying the AM2.1 distribution of SAF versus effective snow albedo yields a very

similar distribution. However the snow albedo values for the AM2.1 runs are generally lower

than that in the CMIP3 models. Specifically, the AM2.1 high run and the CM2.1 snow albedo

value are not the same. Recall from Chapter 2 that the AM2.1 high run is the standard albedo

level, meaning that it was not perturbed and should therefore have the same albedo to that in the

CM2.1 run. However the CM2.1 snow albedo value in the 20th Century is 0.54 while in the

AM2.1 high albedo scenario the value is 0.50. Colder models will tend to have a larger snow

cover fraction and therefore would yield a higher surface albedo. This is assumed because colder

environments are more conducive to snowfall and thus snow covered regions. Of importance

however, is the fact that the spread in SAF shown by the CMIP3 models can be produced by the

AM2.1. The AM2.1 simulations can now be used as a sensitivity analysis to evaluate the role of

SAF on other variables.

The correlation between SAF and snow albedo shown in Figure 3.8 indicates that models

with higher snow albedo will exhibit stronger SAF while models with a lower snow albedo will

exhibit weaker SAF strength. It has been explored by Levis et al. (2007) that climates with

higher albedo tend to be colder and will have a greater mass of snow to melt from one time

period to another. The larger change in snow contrast will allow for more incoming solar

radiation to be absorbed by the ground. This will amplify the ambient temperature and hence

explains why the SAF strength would be stronger.

The results in this section established the fact that the AM2.1 can replicate the spread in

SAF by perturbing the snow albedo that was seen in Qu and Hall, (2006), Figure 3.8. Models

with higher snow albedo exhibits stronger SAF. This indicates that snow albedo is a good

indicator of the SAF response which is evident in both simulations of the CMIP3 and AM2.1

runs. CM2.1 has a colder bias than AM2.1 and colder models generate stronger SAF. This is verified by the results from Levis et al. (2007) who showed that models with higher snow albedo are generally colder with a greater surface warming response to climate change. Further inquiry will now seek to determine the knock-on effects related to SAF using the CMIP3 models and the AM2.1 simulation runs.
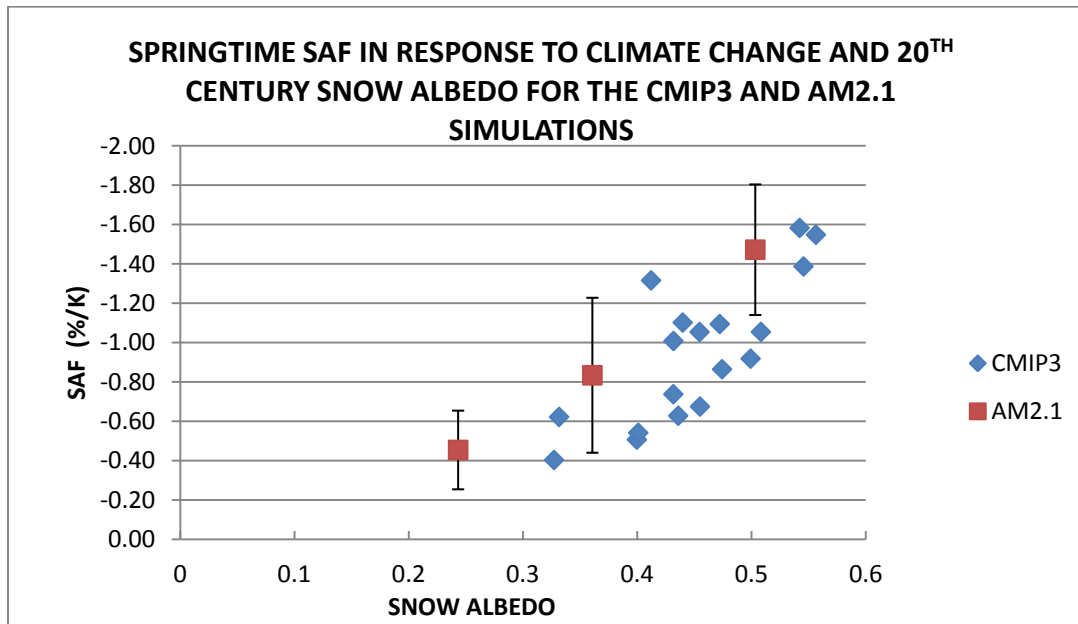
Figure 3.8: Relationship between MAM SAF (%K^{-1}) and present day snow albedo for areas polewards of 30° North, with grid cells greater than 10% snow cover for 18 GCMs and the AM2.1 simulation runs.
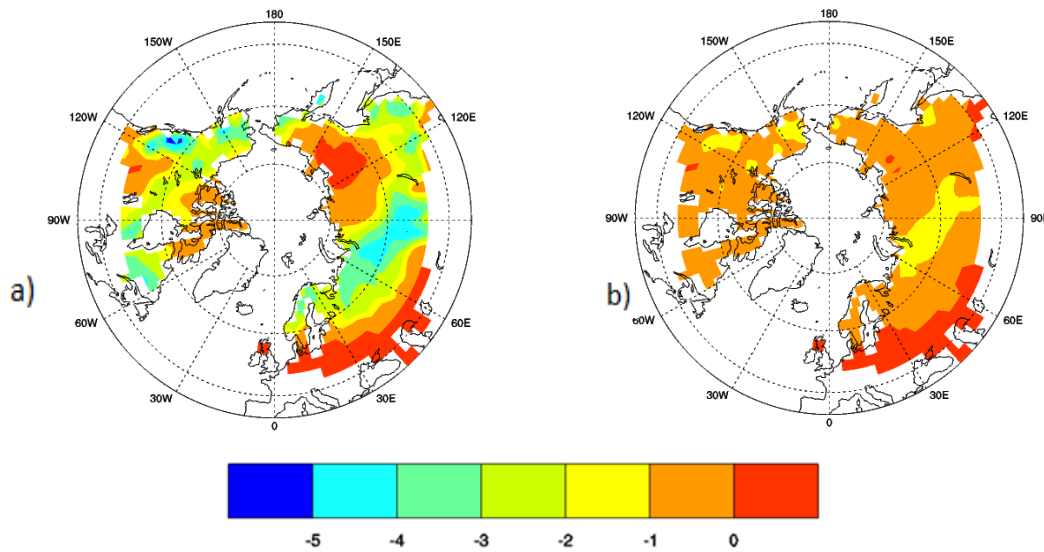
Figure 3.9: Springtime SAF (%K^{-1})for land areas polewards of 30° North for grid cells greater than 10% snow cover in the AM2.1 simulation run for (a) high albedo and (b) low albedo run.

3.4 Summertime Knock-On Effects Associated with SAF

In this section, the summertime soil moisture, springtime snow mass and snowmelt response to SAF will be assessed using the CMIP3 models and the AM2.1 runs. The question that is posed is whether the AM2.1 simulation can produce the knock-on effects associated with SAF.

Figure 3.10 shows the springtime SAF with respect to the mean change in summertime soil moisture in response to climate change among the CMIP3 models. The CMIP3 models show that as SAF increases (in magnitude) the soil moisture decreases. The negative correlation among the mean change in soil moisture is weak at 0.43. Furthermore the correlation is not statistically significant with a P value of 0.11 at the 95% a confidence level. Hall et al. (2008), however,

found that the correlation between SAF strength and changes in summertime soil moisture to be -0.8. The stark contrast in this investigation's results relative to that of Hall et al., (2008) could be attributed to the spatial area investigated. This research takes into account the land areas between 30° and 90° North while Hall et al., (2008) conducted their research over the United States. Nevertheless, Hall et al., (2008) found that models with stronger SAF are associated with less springtime snow packs and therefore less snowmelt. Figure 3.11 shows the response of the mean change in springtime snow mass with respect to springtime SAF in response to climate change for the CMIP3 models. This shows that models with stronger SAF will also exhibit a greater reduction in snow mass with a significant correlation coefficient of -0.61 with a P value of 0.009 at a 95% confidence level. Figure 3.12 shows that models with a stronger SAF will also exhibit a greater decrease in snowmelt from the 20$^{\text{th}}$ to the 21$^{\text{st}}$ Century. If the change in snow mass decreases, it is anticipated that snowmelt will also decrease for models with stronger SAF, Figure 3.12. However Figure 3.12 shows a weak negative correlation which is not statistically significant.

Based on these results generated from the CMIP3 models, no conclusive results between springtime SAF and summertime soil moisture along with changes in snowmelt can be determined. However, there is a significant correlation between springtime SAF and snow mass, although these correlations were established in previous literature such as by Hall et al. (2008). The next step attempts to determine whether these knock-on effects can clearly be generated in a controlled environment, using the AM2.1 simulation.
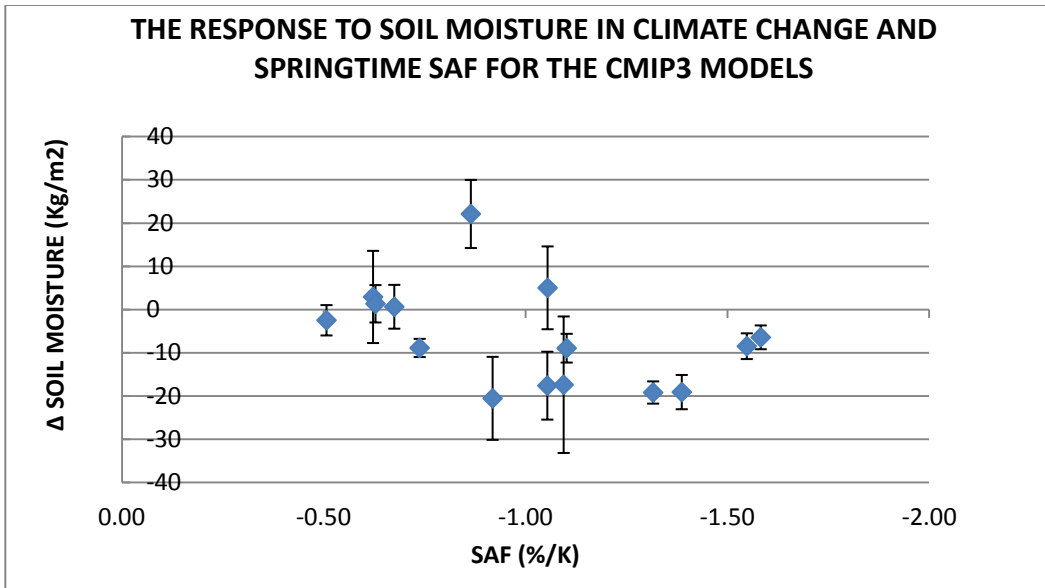
Figure 3.10: Change between the 20th and 21st Centuries mean JJA soil moisture (kgm^{-2}) for land areas polewards of 30° North with respect to MAM SAF (%K^{-1}) for the CMIP3 models.
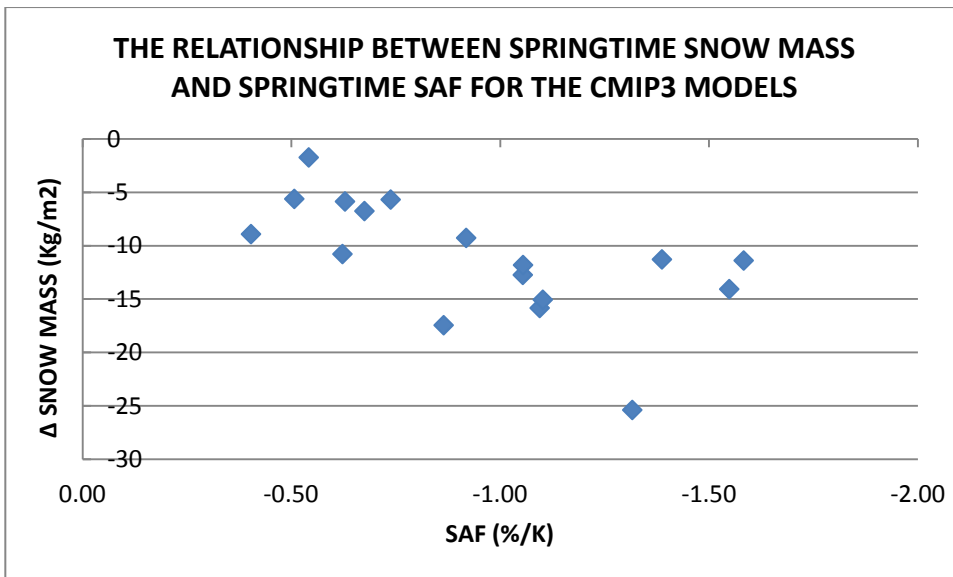
Figure 3.11: Change between 20th and 21st Centuries mean JJA snow mass (kgm^{-2}) for land areas polewards of 30° North with respect to MAM SAF (%K^{-1}) for the CMIP3 models.
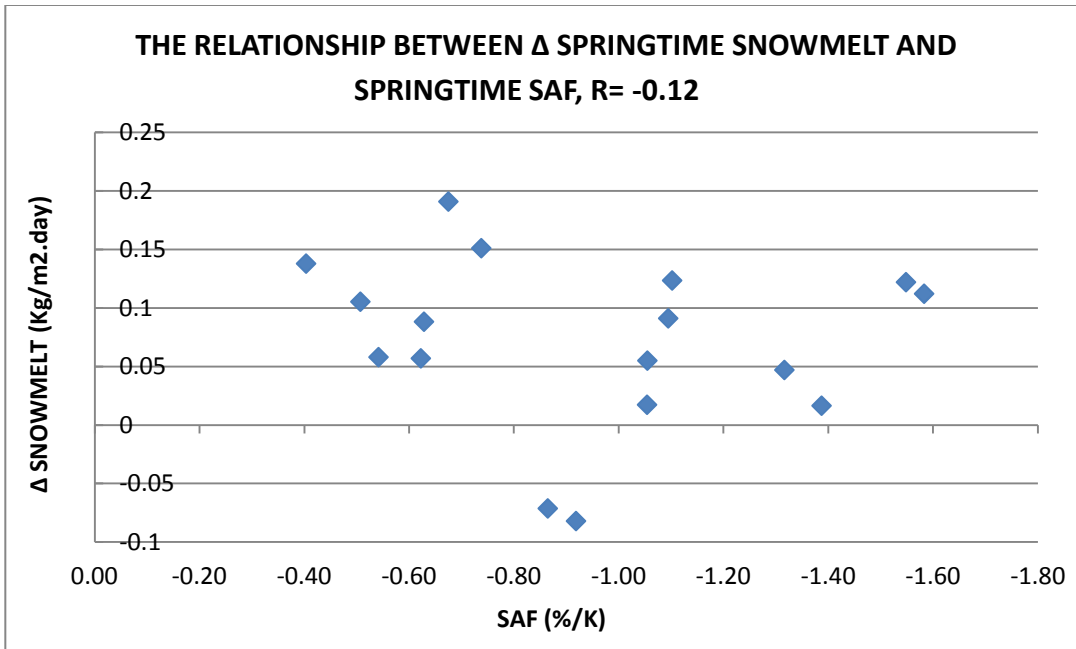
Figure 3.12: Change between 20th and 21st Centuries mean JJA snowmelt (kgm^{-2}.day) for land areas polewards of 30° North with respect to MAM SAF (%K^{-1}) for the CMIP3 models.

The monthly changes in soil moisture in response to climate change for the AM2.1 runs are plotted as in Figure 3.13. This distribution illustrates that the largest drying among the runs occurs in the summer months of May, June and July. It is expected, based on work conducted by Hall et al. (2008) that models with stronger SAF would have a larger summertime drying. However Figure 3.13 shows that during the summer months, the high albedo run, (indicative of the strongest SAF) does not produce the largest drying, but rather lies in between the low and middle runs. Furthermore, the standard deviation shows that there is no significant difference between the high, mid and low AM2.1 runs. Therefore no conclusive observation can be made on whether the soil moisture among the three runs can reproduce the features seen in the CMIP3 models.

To verify the results, the investigation also examines the snow pack mass and snow melt response to climate change in the AM2.1 simulation. This will help decipher whether the results follow the same distributional pattern seen in the Figures 3.11 and 3.12 respectively. The

snowpack and snowmelt response to climate change follow the same patterns as that seen in the CMIP3. That is, the highest albedo run, exhibits the greatest change in snow mass and snowmelt in response to climate change. However, the values among these runs are not statistically significant and hence, no robust conclusion can be made. Therefore it cannot be concluded that the different springtime SAF will produce significantly different soil moisture and snowmelt in response to climate change using the AM2.1 runs.
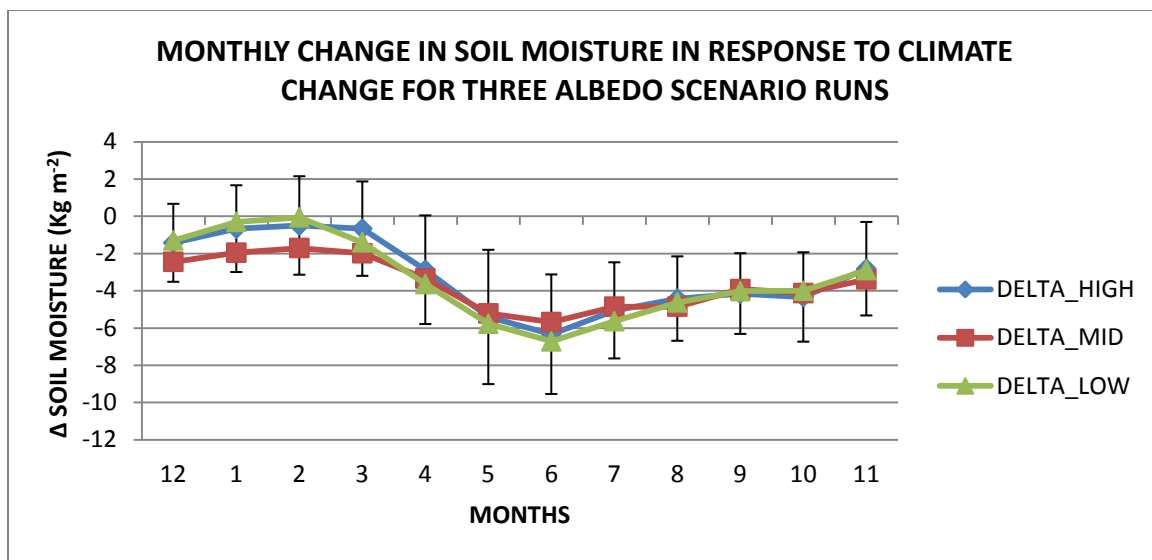
Figure 3.13: Monthly changes in soil moisture (kgm^{-2}) between the 20th and 21st Centuries polewards of 30° North for the high (blue), middle (red) and low (green) AM2.1 snow albedo scenarios.
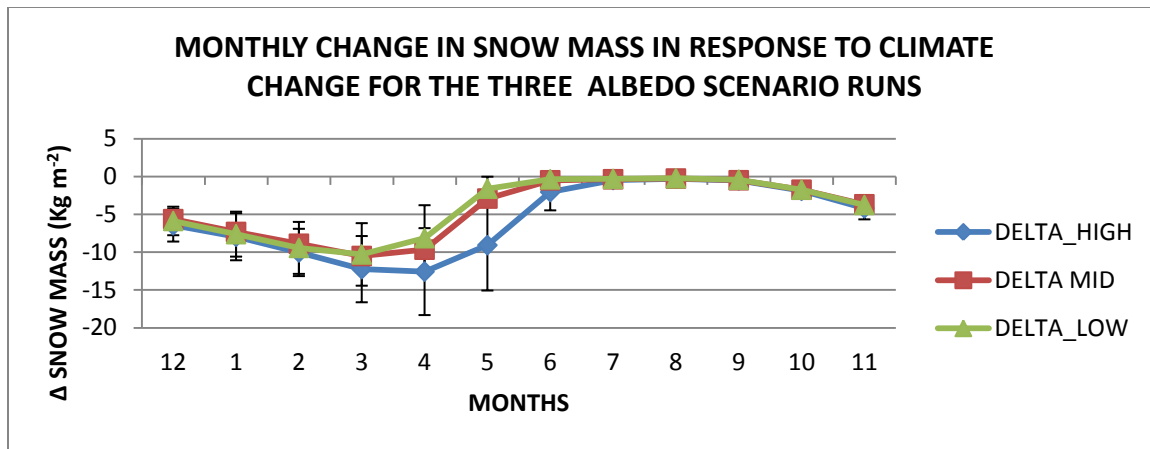
Figure 3.14: Monthly changes in snow mass (kgm[-2]) between the 20th and 21st Centuries polewards of 30° North for the high (blue), middle (red) and low (green) AM2.1 snow albedo scenarios.
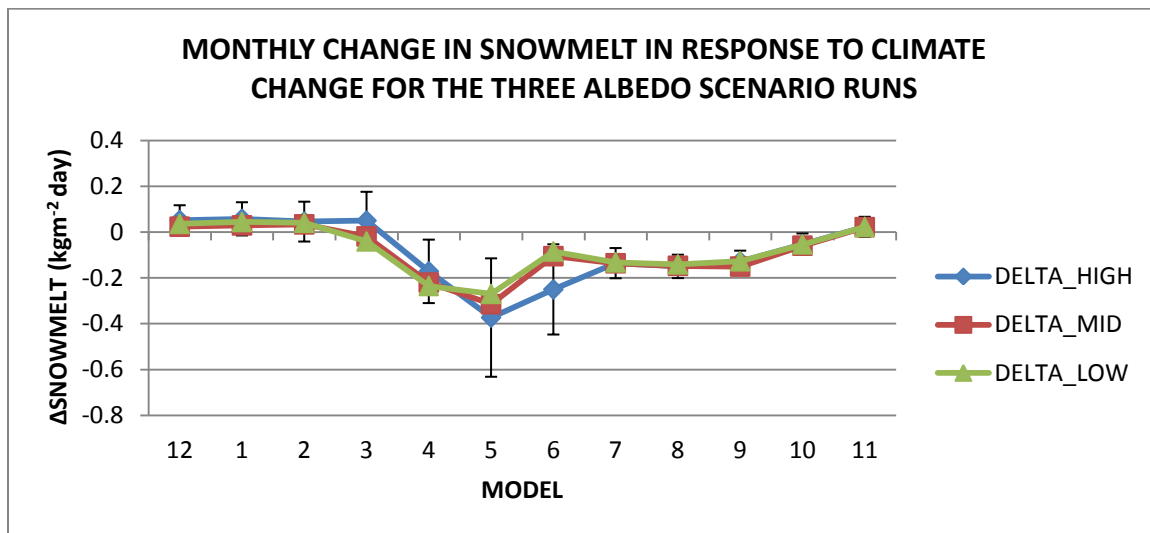
Figure 3.15: Monthly changes in snowmelt (kgm[-2].day) between the 20th and 21st Centuries polewards of 30° North for the high (blue), middle (red) and low (green) AM2.1 snow albedo scenarios.

3.5 Summary

This chapter tested whether a series of sensitivity analyses in perturbing snow albedo in an uncoupled model, AM2.1, from low to high could reproduce the spread in SAF together with

the components associated with SAF. This was conducted by using the AM2.1 simulation to investigate the variables influencing SAF along with the main components influencing SAF in the low to high albedo runs. The AM2.1 simulations successfully reproduced the spread in SAF exhibited by the CMIP3 models as well as the two factors, SNC and TEM influencing SAF.

The CMIP3 and AM2.1 models were also used to explore the knock-on effects associated with SAF in response to climate change. The CMIP3 models could not reproduce a significant correlation between springtime SAF and summertime changes in soil moisture as well as that of snowmelt, which were evident in previous literature. However there was a significant correlation between springtime SAF and snow mass. The AM2.1 then tested whether the knock-on effects could be produced in a controlled environment without the influence of external climate influences. However, the AM2.1 results produced inconclusive results of the summertime soil moisture, snow mass and snow melt with respect to springtime SAF.

CHAPTER 4 CIRCULATION

This chapter explores the relationship between springtime SAF and the summertime circulation patterns. The temperature response to climate change is more significant over land than ocean and thus a temperature gradient is produced. Recall from Section 1.1.3 that LSC is defined as the thermal heat contrast between the land and ocean $\frac{dT}{dx}$. The LSC will also change in response to climate change, $\frac{dT}{dx}(dt)$, here on in denoted as dLSC. This chapter tests the hypothesis which states that models with stronger SAF will exhibit a stronger summertime dLSC. Investigations will be conducted to test whether dLSC is the mechanism that contributes to the summertime circulation patterns (Fletcher et al., 2009).

A series of investigations are conducted using the CMIP3 models, to test the aforementioned hypothesis. The variables used in this investigation are the change in surface temperature and Sea Level Pressure in response to climate change, $\frac{dT}{dt}$ and $\frac{dSLP}{dt}$, which are denoted as dT and dSLP respectively. Recall that the response to climate change is taken as the difference between the mean of the last 20 years for the 20th and 21st Centuries. First, a number of scatter plots are produced to show the relationship between SAF and dTland; SAF and dTocean and SAF and dLSC. Once the relationship between SAF and dLSC is determined, then regression plots are created to investigate the relationship between springtime SAF and summertime circulation, as well as summertime dLSC and the summertime circulation patterns. These regressions plots are then compared.

Furthermore, the summertime circulation response to SAF in climate change is compared to that generated by the AM2.1 uncoupled model to establish whether the AM2.1 can reproduce

the same summertime circulation features exhibited by that of the CMIP3 models. Finally this chapter will quantitatively determine whether the summertime circulation patterns exhibited by dLSC are influenced by springtime SAF.

4.1 Summertime Circulation Response to SAF (CMIP3)

In this section summertime dT and dSLP are investigated with respect to springtime SAF. The dT and dSLP are regressed on SAF for all land and ocean areas polewards of 30°N, Figures 4.1(a) and (b). The shaded red and blue areas represent positive and negative correlation respectively between the circulation variables of dT and dSLP, on SAF. The regions shaded in red signifies that models with stronger SAF will exhibit a stronger response to surface warming in Figure 4.1(a), and an increase in surface pressure, Figure 4.1(b). The regions shaded in blue indicate that as SAF increases among the models, the surface temperature and sea level pressure will decrease. Figure 4.1(a) shows that the warm continental surface temperature is spread zonally to encompass all of Eurasia. The colder temperatures are confined to a small area over the Northern Pacific and Atlantic Ocean due to the increase in summertime heating. As a result, the dSLP increases over these ocean bodies and decreases as dLSC increases over most of the NH continental regions, Figure 4.1(b). The stippled regions show where the relationships between the variables are significant with a 95% confidence level. There is significant zonal warming over the Northern United States and the Northeastern Pacific Ocean. Also there is significant warming in regions over mid Eurasia in the Middle East to Kazakhstan and out towards Mongolia and Northeastern China. As dT increases over the landmasses, the dSLP decreases over the corresponding areas. This is expected as increased insolation enhances

radiative forcing, therefore, inducing surface convergence and the vertical rising motion of air, thus, reducing the surface pressure. The circulation patterns are in agreement with Fletcher et al. (2009) who explained that SAF is associated with summertime nonlocal circulation patterns. They show that the increase warming response is predominant over the Northern Hemisphere's midlatitudes where SAF is expected to amplify surface temperatures from the initial anthropogenic warming.

Fletcher et al. (2009) further showed that the surface warming response to climate change is larger for models with stronger SAF. Their work along with this current research agree with Hall et al. (2008) who suggested that the strongest warming response is located over the continental United States where a negative trend in springtime snow cover is largest (Groisman et al., 2004). Fletcher et al. (2009) also observed that a similar, but weaker, temperature response is prevalent over Eurasia. They attribute this to less drying over a large region of Eastern Eurasia which is indicative of more evaporative cooling that causes a weaker positive temperature feedback. Contrary to this is the response over Central North America where there is more drying and therefore less evapotranspiration, thus increasing sensible heat and causing a stronger positive temperature feedback. Furthermore, Fletcher et al. (2009) showed that surface responses associated with SAF are weak over the Arctic basin, suggesting that SAF is not related to surface warming or circulation changes in this region. They show that there is significant warming over the North Pacific with opposite-signed anomalies of sea level pressure for the northern oceans and the continents. Their results indicate that models with stronger SAF induce rapid warming over the land as opposed to that over the ocean.

Figure 4.1(b) shows dSLP regressed on SAF. This figure shows a distinct decrease in sea level pressure over landmasses and increase over the oceans. This corresponds to increase

warming relative to stronger SAF over landmasses and cooling relative to stronger SAF over the oceans in response to climate change. It is expected that the increase surface warming that is associated with SAF, induces surface convergence over the land and divergence over the oceans, therefore inducing lower surface pressure over continental regions and higher pressure over oceans. This also inevitably induces upper level circulation patterns.

Models with stronger SAF are associated with mid-tropospheric warming at 50°North, with a dipolar wind response that peaks in the upper troposphere which is in thermal wind balance with the warming (Fletcher et al., 2009). Furthermore, Fletcher et al. (2012) suggested that the geopotential response to increased vertical warming throughout the troposphere is evident in regions between 40° to 60°N where SAF is predominantly the strongest. They also suggest that SAF is linked to zonal –mean response of the atmospheric circulation and the zonal-mean response to a polewards shift of the subtropical jet.
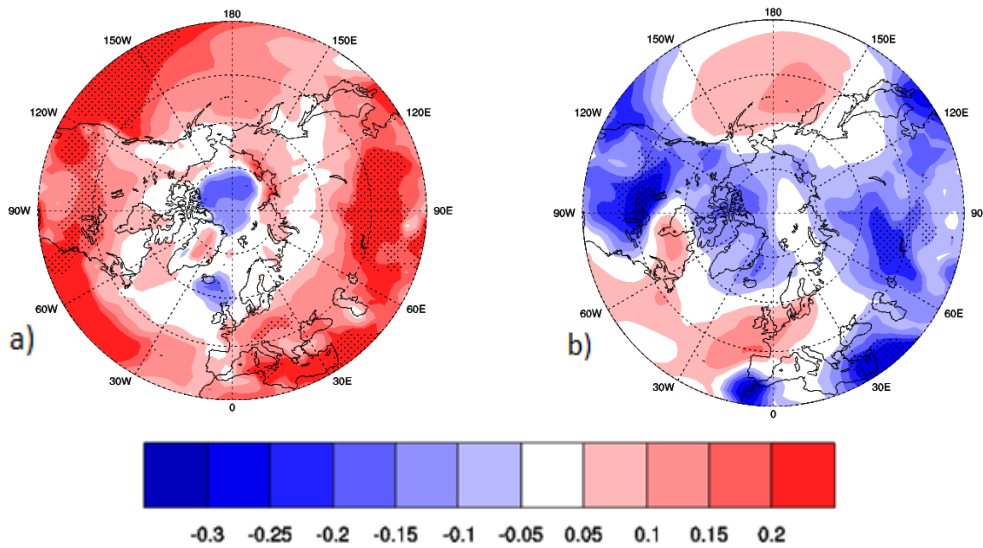
Figure 4.1: The mean JJA change in 20th and 21st Centuries (a) surface temperature regressed on SAF in units of $(K^2\%^{-1})$, (b) sea level pressure regressed on SAF $(hPa.K.\%^{-1})$.

4.2 SAF and the Thermal Land Sea Contrast

The aforementioned results show that models with stronger SAF will yield a greater warming response to climate change. Speculations into the different heat capacities of landmasses and oceans suggest that a stronger response to warming in climate change occurs predominantly over land than over ocean. Figure 4.2 examines the dTland and dTocean separately with respect to SAF. It shows that models with stronger SAF exhibit stronger dTland and dTocean with an r value of 0.5 and 0.3 respectively. However, it is evident that dTland is greater than that of dTocean. If the land and ocean temperatures change in response to climate change, then LSC will also change in response to climate change (dLSC), because the land and oceans do not warm at the same rate.
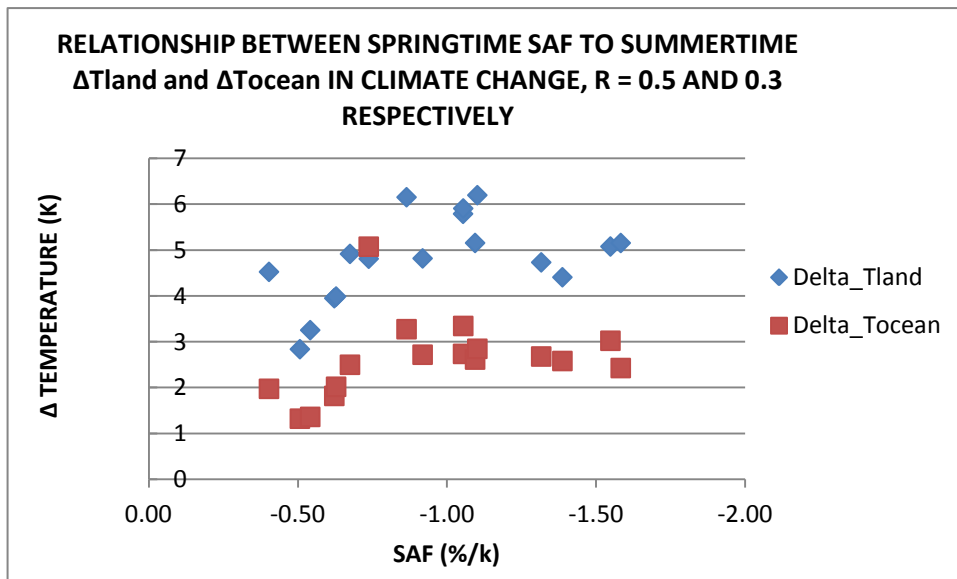
Figure 4.2: Change in mean JJA land surface temperature and SST between the 20th and 21st Centuries with respect to MAM SAF.

The question now arises as to whether there is a relationship between springtime SAF and summertime dLSC. This could give a potential explanation to the circulation patterns seen in Fletcher et al. (2009). It is evident that models with stronger SAF exhibit stronger dLSC, Figure4.3. However, the correlation is weak with an r value of 0.24. The r^2 value is 0.057 and indicates that 6% of the variation in dLSC can be explained by SAF. However, the Pvalue is 0.35 which is greater than the 0.05, testing at the 95% confidence level. Therefore the relationship between springtime SAF and summertime dLSC is not significant.
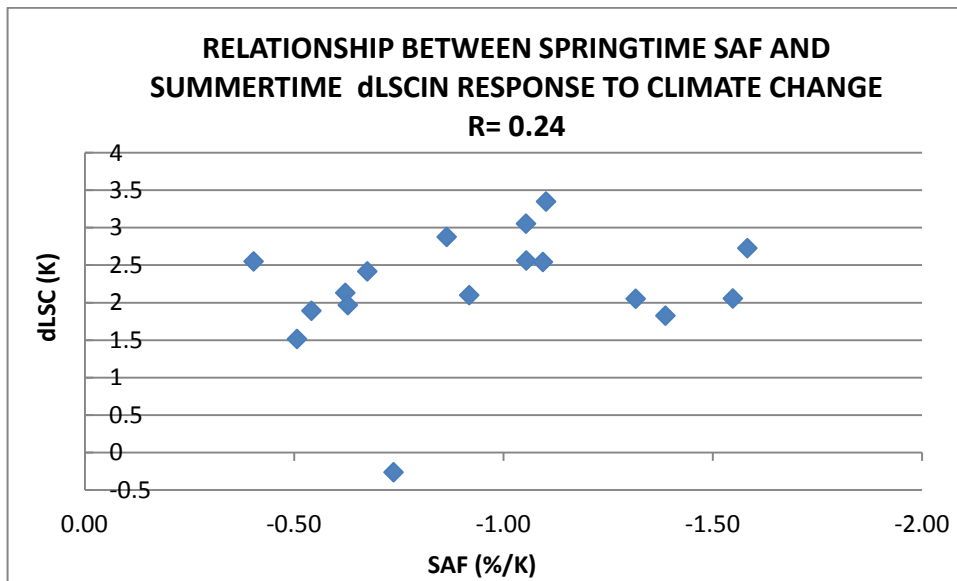
Figure 4.3: Relationship between the change in summertime Land Sea Contrast (dLSC) between the 20th and 21st Centuries and springtime SAF.

The aforementioned results show that SAF is associated with circulation response under climate change, which is also seen in Fletcher et al. (2009). The research results also show that springtime SAF is weakly associated with summertime dLSC. From previous literature, it is apparent that LSC is associated with circulation patterns. In summer, models with strong LSC are more conducive to larger and lower level energy transport from oceans to land in order to

facilitate the energy mass momentum balance. According to Fasullo, (2010), LSC plays a prominent role in the changes in the energy flow through the climate system and contributes to equilibrating the planetary energy balance. This research seeks to now investigate whether dLSC is linked to the summertime circulation response to climate change and whether the circulation response is similar to those influenced by SAF.

The purpose of investigating the influence of dLSC on circulation is to differentiate whether the circulation patterns seen are similar to those observed in Fletcher et al. (2009). If the results are similar, then this would indicate that dLSC is a physical mechanism that contributes to the circulation patterns and which is further related to the influence of SAF. If it is not, then the atmospheric circulation response to dLSC and, dLSC to SAF are not necessarily linked.

To investigate the relationship between dLSC and the summertime circulation response to climate change, polar stereographic maps are created where dT is regressed on dLSC, Figure 4.4(a). This shows that the areas of significant warming occur predominantly over Eurasia and the Western Atlantic Ocean. In Eurasia the significant warming is prevalent in the Middle East and Northern China. This spatial distribution is similar to that of dT regressed on SAF, recall Figure 4.1(a). Both Figure 4.1(a) and Figure 4.4(a) are similar in that significant warming occurs over the Middle East and Northern China. However, they differ in the Western Hemisphere. While Figure 4.1(a) shows significant warming over the interior continent of North America, Figure 4.4(a) offsets this significance stippling to the Western Pacific with no significant warming over North America. There is also no significant warming over the Northeastern Pacific Ocean, Figure 4.4(a), which is also evident in Figure 4.1(a). Furthermore, significant cooling is evident in the Eastern Atlantic Ocean, with cooling also seen in the Pacific Ocean for Figure 4.4 (a). This is not spatially represented in Figure 4.1(a). Overall it is more obvious in

Figure 4.4(a), that there is a clearer delineation between ocean and land temperature response to climate change than dT regressed on SAF in Figure 4.1(a). Finally the positive and negative correlations are stronger in Figure 4.4(a) than in Figure 4.1(a). Specifically, with regards to North America, it is evident that springtime SAF is more influential on the summertime response to dT than dLSC. For areas around the Middle East and Northern China, both SAF and dLSC influence the dT.

The similarities between Figure 4.1(b) and Figure 4.4(b) are however, less apparent than with dT. Figure4.4 (b) shows the regression of dSLP on dLSC. There is a positive correlation in the Atlantic Ocean with significant correlations over the Maritimes and Atlantic Provinces as well as over Ireland and the United Kingdom. However in comparing these observations seen in Figure 4.1(b), where dSLP is regressed on SAF, differing characteristics are quite apparent.
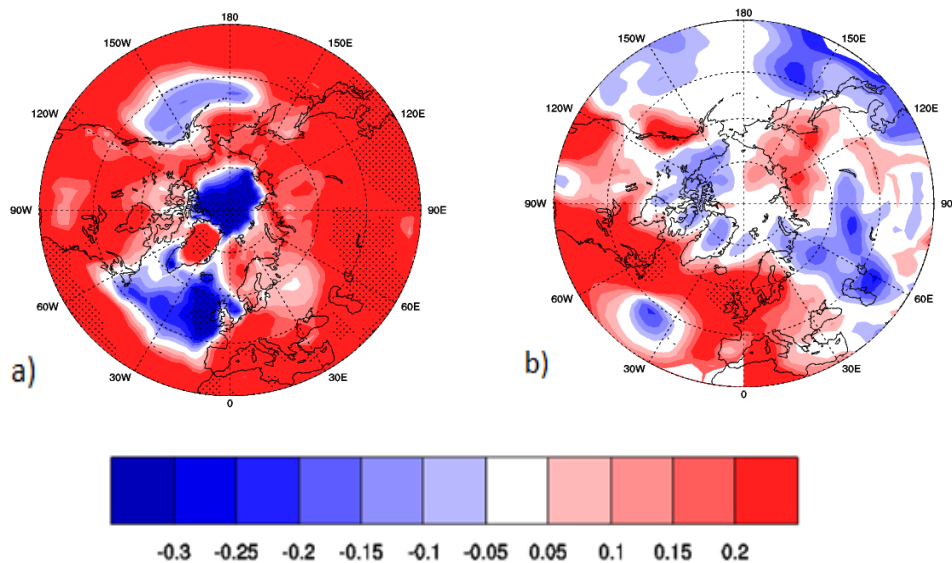
Figure 4.4: The mean JJA change in 20th and 21st Centuries (a) surface temperature regressed on dLSC in unit less), (b) sea level pressure regressed on dLSC (hPaK^{-1}).

Figure 4.4(b) does not show any distinct pattern in the Eastern Hemisphere of dSLP regressed on dLSC. In Figure 4.1(b) there is a clear negative regression coefficient dominating over landmasses and positive correlation prevalent over oceans. In Figure 4.4(b) the spatial distribution of dSLP on dLSC is not easily delineated as dSLP regressed on SAF, therefore, the circulation patterns seen in Figure 4.4(b) show differences from that in Figure 4.1(b).

4.3 Circulation Patterns in the AM2.1 Simulations

The previous sections investigated the response of dT and dSLP to SAF using coupled GCMs. However investigations that are conducted in the coupled GCMs on circulation response related to SAF can generate results that are influenced by other climate components such as heat energy fluxes from the oceans that are not related specifically to SAF. As mentioned in Section 4.1, dLSC may be attributed to various factors. Therefore in this section, the research turns to a more controlled approach to test the circulation patterns related to SAF. This is performed by keeping the ocean prescribed and only perturbing the snow albedo in the AM2.1 simulation. The panel of polar stereographic maps presented in Figure 4.5 shows the circulation response to SAF when ocean temperatures are prescribed and only snow albedo is perturbed in the 20th and 21st Centuries.

Figure 4.5(a) shows the change in surface temperature in response to changes in snow albedo for 20th Century denoted as dTα20. This is calculated for the summertime surface temperature by computing the difference from the high to low springtime albedo runs for the 20th Century. Canada, excluding the Maritimes and Atlantic Province, is sensitive to increase in effective snow albedo which results in a larger decrease in surface temperature and a cooling of

73

over 0.3°C. The strong cooling is also recognized over Eastern Russia and areas over

Kazakhstan, eastward to Mongolia. This indicates that as the snow albedo is perturbed from low

to high, these areas are most affected and thus exhibit the strongest cooling.
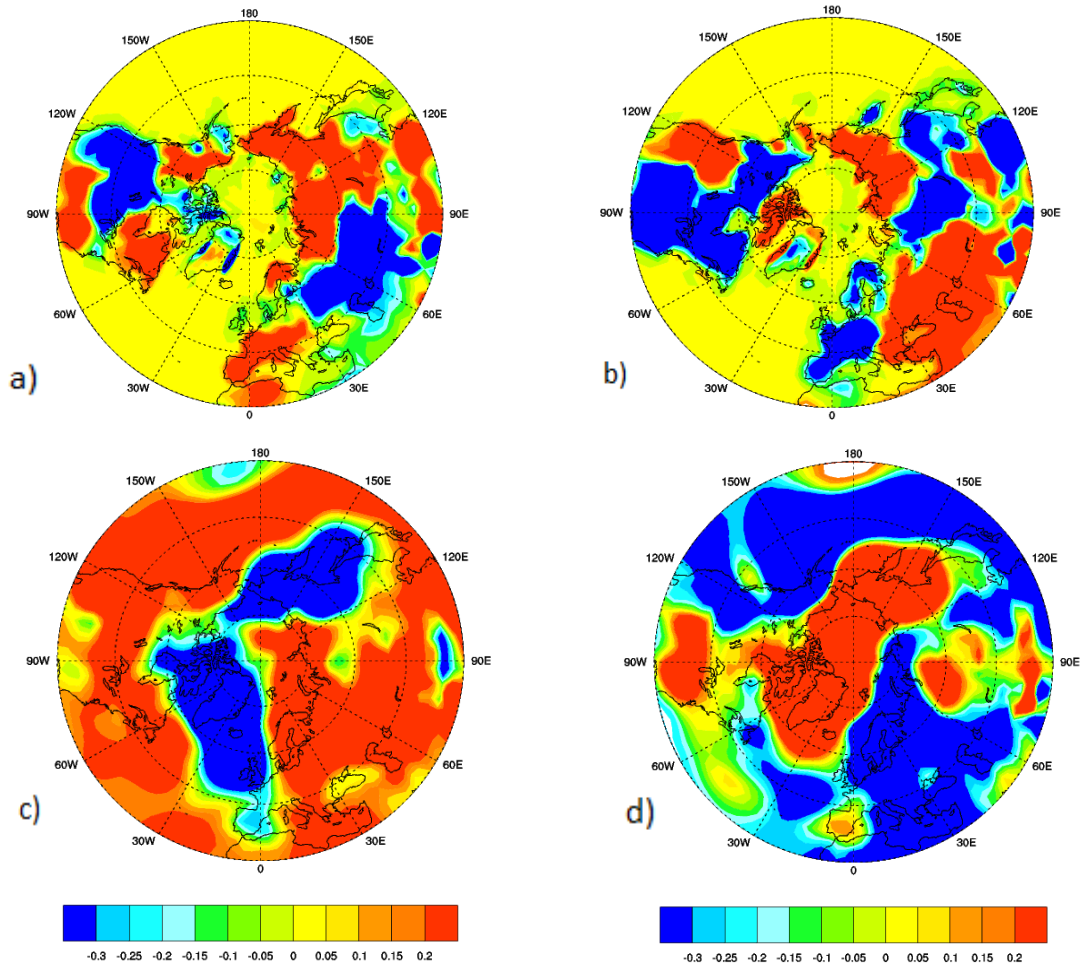
Figure 4.5: Difference between the mean JJA, 20th Century high and low albedo for (a) surface temperature (Kelvin) and (c) sea level pressure (hPa). (b) Difference between the mean JJA high and low albedo in response to climate change (20th and 21st Centuries) for surface temperature and (d) sea level pressure.

The Lower Atlantic and Gulf Coast States in the United States, along with Siberia, exhibit surface warming. This indicates that as the snow albedo is perturbed from low to high, these regions exhibit a strong increase in surface temperature. Recall from Chapter 3, Table 3.1 that the high albedo run in the AM2.1 yields colder surface temperatures than the lower albedo run in both centuries. Models with higher albedo and more snow cover will reflect a larger fraction of incoming solar radiation therefore, keeping the surface cool. Thus, the difference between the high minus the low albedo surface temperatures should be negative as a result of this research findings. Assuming that this is what is most likely expected when perturbing the effective snow albedo from low to high, it is not obvious as to why areas of Siberia and the Lower Atlantic and Gulf coast States show areas of warming. However since it is now established that different areas respond differently to perturbations in snow albedo, it will be interesting to investigate how these changes in surface temperature due to perturbations in snow albedo will respond to climate change, and whether these changes in surface temperature will be similar to those generated from the CMIP3 models.

Figure 4.5(b) shows the difference between $dT\alpha21$ and $dT\alpha20$. It shows the regions that are most sensitive to changes in snow albedo in response to climate change, $dT\alpha$. The sensitivities over the regions are determined by the magnitude of the resultant change between $dT\alpha21$ and $dT\alpha20$. The negative values of $dT\alpha$ indicate that $dT\alpha21$ is less than $dT\alpha20$, which implies that the change in surface temperature as a response to perturbations from effective snow albedo in the 20th Century is greater than the changes seen to that in the 21st Century. Figure 4.5(b) illustrates a stronger change in temperature occurring over Western Eurasia and Western North America where $dT\alpha21$ is larger than $dT\alpha20$. Therefore the surface temperature warms stronger in the 21st Century than in the 20th Century over these regions. This shows similarity to

that generated in the fully coupled models. These areas correspond to those that show a significant warming in Figure 4.1(a). The areas that respond similarly in the AM2.1 and CMIP3 are the Pacific Coast of North America and areas around the Middle East, Eastward to Mongolia. Therefore, the AM2.1 simulation shows similar spatial responses of surface temperature to those seen in the CMIP3 simulation which is evident from visually observing and comparing Figure 4.1(a) and Figure 4.5(b).

As mentioned earlier in this chapter, changes in surface temperature will induce perturbations in surface pressure which drives circulation. Here the sea level pressure is also examined as that of $dT\alpha$. Most of the continental regions indicate a strong increase in sea level pressure in the 20th Century as a result of perturbing snow albedo from low to high. The positive $dSLP\alpha$ also corresponds to areas where decreasing surface temperature occurs as in the Northern Atlantic and Northern Siberia regions. Note that in Figures 4.5(a) and (b), there are no changes in ocean temperatures. This is because the ocean temperature remains constant in the albedo runs and do not respond to changes in the atmosphere nor on land. However, for the sea level pressure, higher levels dominating over the continental areas will induce lower pressure systems to occur over the oceans and hence the circulation pattern seen in Figure 4.5(c).

This circulation response differs in response to climate change Figure 4.5(d). The Northern Atlantic and Northeastern Siberia are regions that exhibit a greater change in surface pressure in the 21st Century, while areas over Eastern Eurasia and the Northern Pacific exhibit a decrease in $dSLP\alpha$ from the 20th to the 21st Centuries. Comparing the circulation response of Figure 4.5(d) to that in Figure 4.1(b), the AM2.1 shows a similar zonal pattern around the 60°N latitude mark. The pattern shows higher pressure straddling the Arctic Basin in both the North Atlantic and North Pacific with lower pressure over the continents. Through visual examination,

it seems apparent that the AM2.1 simulation can also, similarly, capture the response of circulation patterns to perturbations in snow albedo in climate change, as presented in the CMIP3 models.

4.4 Summary

In this chapter a number of results were presented to test whether models with stronger springtime SAF show stronger summertime dLSC in response to climate change. The research tested whether dLSC is a physical mechanism that contributes to the summertime circulation response patterns seen in Fletcher et al. (2009). By regressing summertime dT and dSLP on springtime SAF the results were similar to those produced by Fletcher et al. (2009). The relationship between circulation on SAF and dLSC were also investigated. The circulation variables were regressed onto dLSC to determine if there were any similarities of the circulation response between the two components, SAF and dLSC. The circulation patterns exhibited between the two components mostly differ except for subtle similarities.

By comparing the circulation response regressed on SAF and on dLSC, there are similar spatial circulation patterns however, circulation patterns regressed on dLSC do not well reproduce the circulation patterns seen by springtime SAF. Models with stronger springtime SAF influence the summertime dLSC. It is noted that 6% of the variation in dLSC can be explained by SAF. The correlation between springtime SAF and summertime dLSC is 0.24, and although there is a slight positive correlation between the two variables, this relationship is not significant. Therefore springtime dLSC is not a physical mechanism that robustly influences the response to

summertime circulation patterns in climate change. This may explain why the spatial circulation patterns are not identical between SAF and dLSC.

To minimize the influence of other climatic factors on circulation, experiments were conducted with the AM2.1 simulation to test whether circulation patterns seen in the CMIP3 models regressed on SAF can be replicated in the AM2.1. Through visual examination, it seems evident that the AM2.1 simulation can similarly capture the circulation patterns in response to perturbations in snow albedo in the climate change, as presented in the CMIP3 models. AM2.1 simulation also shows similar spatial responses of surface temperature and sea level pressure to those seen in the CMIP3 simulation.

CHAPTER 5 CONCLUSION

5.1 Research Summary

The anthropogenic warming of climate change has implications on all components of the climate including snow covered regions. The changes of snow cover and snow albedo in these regions induce SAF which amplifies the climate warming response to the increased atmospheric CO_2 concentrations. There is a large spread in SAF among the 17 CMIP3 models and this is primarily due to the model's snow albedo. It has also been established that springtime SAF has implications on springtime snow mass and snowmelt, as well as summertime soil moisture, surface temperature, sea level pressure and circulation patterns in response to climate change. Limited conclusive results linking SAF to these responses were conducted in previous studies.

This research analyzed springtime SAF in two parts. The first conducted a set of numerical sensitivity experiments using the Atmospheric Model 2.1 (AM2.1) simulation to probe the factors contributing to SAF as well as the knock-on effects influenced by SAF. This was performed by perturbing the snow albedo from low to high and monitoring the response of a number of variables including surface temperature, surface albedo and snow cover fraction in both the 20th and 21st Centuries and in response to climate change. These results were then compared to those generated by the CMIP3 models to decipher the similarities and differences between the two simulations.

The second part of the results section focused on the circulation response to SAF, where the CMIP3 models were used to investigate whether summertime Land Sea Contrast in response to climate change (dLSC) is influenced by springtime SAF in response climate change. These

results were then compared to those generated by the AM2.1 simulations to identify similarities and differences in the responses of surface temperature and sea level pressure. These investigations are valuable because they test whether a controlled and uncoupled model can in fact produce similar results to those exhibited by a fully coupled GCM.

Conducting these investigations using the AM2.1 simulation was useful for two reasons. The first, attempted to remove any external factors that may have influenced the variables being tested. Thus by conducting the sensitivity experiments, this allowed only one variable to be perturbed while assessing the response from the other variables. The AM2.1 was used to diagnose the components of SAF and the features associated with SAF in the CMIP3 models. Providing that the AM2.1 successfully generated similar responses to those exhibited by the CMIP3, then the second reason is the reduced time and funding that are required for designing an uncoupled model relative to a coupled GCM. Therefore, investigations into variables influencing SAF, and the knock-on effects to SAF were investigated in Chapter 3 and 4 using the AM2.1albedo runs and the CMIP3 simulations.

5.1.1 Variables Influencing SAF

In Chapter 3 the variables influencing SAF were investigated using both the AM2.1 and the CMIP3 models. Two factors contributing to SAF are SNC and TEM. SNC is the snow cover contrast which represents the albedo contrast of snow-covered and snow-free land. The TEM term represents the change in the snowpack albedo due to snow metamorphosis as a function of temperature (TEM) (Fletcher et al., 2012). In both the CMIP3 and the AM2.1simulations, SNC showed a greater influence on SAF than TEM. This is in agreement with Qu and Hall, (2007)

who compared SNC and TEM among the CMIP3 models. In the AM2.1 high run, the SNC term is on average 32 times larger than the TEM term which indicates that SNC is the dominant component that influences SAF. The reason for the low values of TEM generated by the AM2.1 simulations has not been explored, but has potential for further empirical and theoretical investigations.

The AM2.1 simulation can also successfully reproduce the spread in SAF exhibited by the CMIP3 models. However, the high AM2.1 run produces a lower value of SAF and snow albedo when it is compared to that in the CMIP3, Coupled Model 2.1 (CM2.1) GCM. This is questionable considering that the snow albedo in both the CM2.1 and AM2.1 high run simulations are supposed to be the same because there were no perturbations to the snow albedo performed in the high run. One possible explanation for this is due to the colder bias in the CM2.1 than the AM2.1. Levis et al. (2007) showed that models with greater changes in temperature are associated with higher snow albedo levels, and thus will exhibit stronger SAF. Despite that the values were not being exactly replicated, the AM2.1 runs showed a similar distribution to that of the CMIP3 models, with a significant difference in SAF between the low and high albedo values. By successfully reproducing the spread in SAF from the CMIP3 models, using the AM2.1 runs, investigations into the knock-on effects were then examined.

5.1.2 Knock – On Effects Associated with SAF

The influence of springtime SAF on summertime soil moisture in response to climate change was investigated as a potential knock-on effect to SAF. The relationship between springtime SAF and the summertime change in soil moisture among the CMIP3 models

indicated a weak negative correlation which was not significant. This is contrary to the significant, negative 0.8 correlation which indicated that as springtime SAF increases the summertime soil moisture in response to climate change decreases (Hall et al., 2008). Applying the methods employed by this research, there was no robust relationship found between springtime SAF and the change in summertime soil moisture and snowmelt, in response to climate change using the CMIP3 models. This could perhaps be attributed to the fact that the spatial regime analyzed in this research differed from that of Hall et al. (2008). It is also found that results from the AM2.1 runs did not produce a significant correlation between SAF and the change in soil moisture. In the AM2.1 analysis, the values of the change in soil moisture among the high, medium and low runs were not significantly different.

In conclusion, the AM2.1 runs can successfully reproduce the spread in SAF along with the components responsible for influencing SAF. The AM2.1 cannot effectively produce the knock- on effects to soil moisture, snow mass and snowmelt in responses to climate change. A potential reason could be due to the fact that there were only three albedo values, low, mid and high, which were used to determine a relationship.

5.1.3 Circulation Effects on SAF

Chapter 4 focused on assessing the circulation response to SAF in climate change. It was hypothesized that models with stronger SAF would exhibit a stronger summertime dLSC in response to climate change, and dLSC could therefore be a physical mechanism contributing to summertime circulation patterns seen in Fletcher et al. (2009). First dT and dSLP were separately regressed onto SAF to confirm whether the circulation response seen in Fletcher et al. (2009)

could be replicated by applying the methods used in this research. The response was successfully reproduced where the increase warming response is predominant over the Northern Hemisphere's midlatitudes. These regions are sensitive to the influence of SAF and are expected to amplify surface temperatures from the initial anthropogenic warming (Fletcher et al., 2009). Furthermore, this research showed significant zonal warming over the Northern United States and the Northeastern Pacific Ocean, as well as significant warming in regions over mid Eurasia in the Middle East to Kazakhstan and out towards Mongolia and Northeastern China.

Once the circulation regressed on SAF was successfully replicated, the analysis looked to establish whether a relationship between SAF and dLSC was evident. Springtime SAF causes increase surface warming and because the land surfaces have a higher heat capacity than that of oceans, it is expected that the land temperatures would produce a greater warming than the oceans, thus creating a thermal contrast. This contrast sets up a pressure gradient force which can induce circulation. Thus, dLSC was examined to determine whether a relationship between SAF and dLSC exists and whether dLSC can influence circulation patterns. The circulation variables are regressed onto dLSC and are compared to those regressed on SAF to test for spatial similarities. Comparison analysis showed that the circulation patterns regressed on dLSC do not well reproduce the circulation patterns seen by springtime SAF. The correlation between springtime SAF and summertime dLSC is not significantly correlated, with an r value of 0.24 and a confidence level of 95%. Therefore springtime dLSC is not a physical mechanism that influences the response to summertime circulation patterns in climate change according to this analysis. This explains why the spatial circulation patterns regressed on SAF are not identical to those regressed on dLSC.

In an attempt to remove all external influences of the climate components on the circulation response to SAF, the AM2.1 simulations were used to test whether the circulation patterns seen in the CMIP3 models regressed on SAF could be replicated in the AM2.1. Visual examinations and observations show that the AM2.1 simulations can in fact reproduce similar spatial responses to those seen in the CMIP3 models simulations. From visual observation, it is concluded that AM2.1 can reproduce some of the circulation features such as surface temperature and sea level pressure as seen in the CMIP3 simulations.

5.2 Limitations and Recommendations for Future Studies

The research can be validated in two ways. The first is by comparing the results presented in this research to those from previous work conducted in this field. Figure 3.3 was initially produced by Levis et al. (2007) and was successfully reproduced in this research with some modifications applied to the method. Figures 3.5 and 3.6 as well as Figure 3.8 were also successfully replicated from Qu and Hall, (2007). Finally, Figures 4.2.1(a) and (b) were reproduced from Fletcher et al. (2009). The successful replication of previous work provided the confidence to continue the investigation using the current research methods with the AM2.1 simulation.

The various tools used to perform the experiments constitute the second manner in which the research can be validated. The Program for Climate Model Diagnosis and Intercomparison (PCDMI) was involved in collecting model outputs from leading model centers around the world, a task assigned from The World Climate Research Programme's (WRCP's) Working Group on Coupled Modelling (WGCM). This gives external organizations access to the data and

allows for transparency of the models and its data. Researchers over the past decade have relied

on the CMIP3 models with a great deal of confidence for their research. This is attested to the

fact that the CMIP3 models were used in the IPCC AR4. The CMIP3 multi- model dataset

served the IPCC's Working Group 1 which focused on the atmosphere, land surface, ocean and

sea ice components of the physical climate system. In addition, the data from AM2.1-LM2, a

subset from the CM2.1, was submitted to PCMDI. This data was also used to predict tropical

precipitation and extratropical circulations which are associated with the El Nino-Southern

Oscillation (ENSO). Furthermore, research using the suite of CMIP3 models was conducted by

Fletcher et al. (2012) who compared SAF among the CMIP3 models with that derived from

satellite observations, using the APP-x satellite.

5.2.1 Limitations

It is important to recognize that every research has its limitations. In addition, when the

focus of the research depends solely on models' output, the limitations within the models

themselves need to be considered. Qu and Hall, (2007) stated that the models with the strongest

SAF in the climate change context all have unrealistically strong SAF in the seasonal cycle by

10%-20% and have very high albedos for snow-covered surfaces. They speculated that snow-

covered surfaces where vegetation protrudes in the real world are assigned unrealistically large

albedo values.

Further limitations to the research point to the lack of available data that were required to

investigate soil moisture in the CMIP3 models. It is unclear whether the inclusion of soil

moisture from the models that did not have readily available soil moisture data would have significantly changed the correlation generated by the investigation.

In this study the exploration of SAF is limited to snow covered regions solely over land areas. Snow covered regions over oceans, such as, on glaciers, ice and on Greenland were not considered. This is because it would have been difficult to delineate between what percentage of the reflectivity was from snow and what was from ice. Future work could perhaps conduct a similar except including all snow covered areas, and figure out a method to delineate between the reflectivity over snow and ice covered regimes. These results could then be compared to the following to assess whether a stronger more robust signal is evident.

5.2.2 Future Studies

There are a few questions that arise from this research which can point the way forward to future studies. Relating directly to the results, there is a concern as to why TEM in the AM2.1 simulations are much smaller in value than those generated among the CMIP3 models. Is there a possibility that there is a physical mechanism in the coupled models that allow for TEM to be larger and is this constrained in uncoupled simulation? Also, more statistical analyses may be required to quantify how well the AM2.1 simulation can reproduce the CMIP3 results, however, this is beyond the scope of this research. More importantly however, is that circulation analyses are not limited to the surface.

Next steps should be to expand the circulation variables to winds, and precipitation, inclusive of temperature and atmospheric pressure at different vertical levels. Therefore, tests can be performed both at the surface and aloft to test vertical convective circulation patterns. With a

86

consideration for circulation, it would be interesting to expand the knock-on effects to teleconnection oscillation patterns in order to decipher both the quantitative and qualitative responses of oscillation patterns such as the North Atlantic Oscillation (NAO), Arctic Oscillation, El Nino and La Nina on SAF. Further investigations could include, how SAF, in response to anthropogenic climate change may contribute to Arctic amplification, studied by Chylek et al. (2009). However, based on this body of research it is evident that springtime SAF in response to climate change yields a weak signal to large scale circulation patterns linked to land sea contrast. Therefore, robust findings connecting SAF to these circulation patterns may be unlikely. Furthermore, testing the regional response of surface temperature and SLP in response to SAF could also yield to less direct, more noise and thus inconclusive results. In order to test regional scale responses to SAF, investigations on snow albedo and SAF would have be conducted at smaller scale synoptic and mesoscale levels. Regional scale weather and climate features could be tested by perturbing the snow albedo at a local scale and monitoring the response of lake temperatures, lake effect snow and small scale circulation patterns driven by land and sea breeze. Further knock- on effects at local scales could be tested by analyzing the cyclogenesis response of Alberta Clippers' and Colorado Lows' intensity, duration and trajectories in response to locally induced SAF.

The aforementioned scope of this literature reiterates the importance for investigating the role of SAF in climate change. Not only is it necessary to understand the response of the climate components to anthropogenic climate change, but it is equally important to recognize the embedded positive feedback role in amplifying the response. Feedbacks such as SAF, may not contribute a large percent to the circulation patterns exhibited by dLSC. However, prior to this research it was unknown whether dLSC was an influential factor influencing circulation patterns

in response to SAF. It is the expectation that the findings of this research can hopefully be

utilized in providing a more in depth understanding of SAF among fully coupled GCMs through

tests performed by the uncoupled simulation.

BIBLIOGRAPHY

Ahrens, C. D. (2005). Essentials of Meteorology An Invitation to the Atmosphere. In C. D. Ahrens, Essentials of Meteorology An Invitation to the Atmosphere (p. 41). United States: Thomson Learning, Inc.

Alekseev, V. A. (1998). Modelling of the present-day climate by the atmospheric model of INM RAS "DNM GCM." INM Tech. Rep. N2086-B98, Institute of Numerical Mathematics, Russian Academy of Sciences,208 pp.

Alexander, M.A., Tomas, R., Deser, C., Lawrence, D.M., 2010. The Atmospheric Response to Projected Terrestrial Snow Changes in the Late Twenty-First Century. *Journal of Climate* 23, 6430–6437.

Anderson et al. (2004, March 11). The New GFDL Global Atmosphere and Land Model AM2-LM2: Evaluation with Prescribed SST Simulations , pp. 4641-4674.

Arakawa, L. (1977). Computational design of the basic dynamical processes of the UCLA general circulation model. In General Circulation Models of the Atmosphere (pp. 173-265). New York: Academic Press, Inc.

Bony, S., Colman, R., Kattsov, V.M., Allan, R.P., Bretherton, C.S., Dufresne, J.L., Hall, A., Hallegatte, S., Holland, M.M., Ingram, W., 2006. How well do we understand and evaluate climate change feedback processes? *Journal of Climate* 19, 3445–3482.

Broccoli, A.J., Lau, N.C., Nath, M.J., 1998. The cold ocean-warm land pattern: Model simulation and relevance to climate change detection. *Journal of climate* 11, 2743–2763.

Cess, R.D., Potter, G.L., (1988). A methodology for understanding and intercomparing atmospheric climate feedback processes in general circulation models. *Journal of Geophysical Research*, 93(D7), 8305–8314, and Coauthors, 1991: Interpretation of snow-climate feedback as produced by 17 general circulation models. Science, 253, 888–892.

Chalita, S. A. (1994). The albedo of temperate and boreal forest and the Northern Hemisphere climate: A senitivity experiment using the LMD GCM. *Climate Dynamic*, 10, 231–240.

Chylek, P., Folland, C.K., Lesins, G., Dubey, M.K., Wang, M., 2009. Arctic air temperature change amplification and the Atlantic Multidecadal Oscillation. *Geophysical Research Letters* 36, L14801, doi:10.1029/2009GL038777.

Cox, P.M., Betts, R.A., Bunton, C.B., Essery, R.L.H., Rowntree, P.R., Smith, J., 1999. The impact of new land surface physics on the GCM simulation of climate and climate sensitivity. *Climate Dynamics* 15, 183–203.

Darnell, W. L., W. F. Staylor, S. K. Gupta, and F. M. Denn, 1988: Estimation of surface insolation using sun-synchronous satellite data. *Journal of Climate*, 1, 820–836.

Delworth, T.L., Broccoli, A.J., Rosati, A., Stouffer, R.J., Balaji, V., Beesley, J.A., Cooke, W.F., Dixon, K.W., Dunne, J., Dunne, K.A., 2006. GFDL's CM2 global coupled climate models. Part I: Formulation and simulation characteristics. J*ournal of Climate*,19, 643–674.

Douville, H. J.-F.-F. (1995). A new snow parameterization for the Météo-France climate model. *Climate Dynamics*, 12, 21–35.

Dutra, E., Schär, C., Viterbo, P., Miranda, P.M.A., 2011. Land-atmosphere coupling associated with snow cover. *Geophysical Research Letters* 38, L15707.

Essery, R. M. (2001). MOSES 2.2 technical documentation. Hadley Centre Tech. Note 30, 31 pp.

Fasullo, J.T., 2010. Robust Land–Ocean Contrasts in Energy and Water Cycle Feedbacks*. *Journal of Climate* 23, 4677–4693.

Fernandes, R., Zhao, H., Wang, X., Key, J., Qu, X., Hall, A., 2009. Controls on Northern Hemisphere snow albedo feedback quantified using satellite Earth observations. *Geophysical Research Letters* 36, L21702, doi:10.1029/2009GL040057

Flanner, M.G., Shell, K.M., Barlage, M., Perovich, D.K., Tschudi, M.A., 2011. Radiative forcing and albedo feedback from the Northern Hemisphere cryosphere between 1979 and 2008. *Nature Geoscience* 4, 151–155.

Fletcher, C.G (2012, September), in communication with Dr. Christopher Fletcher

Fletcher, C.G., Kushner, P.J., Hall, A., Qu, X., 2009. Circulation responses to snow albedo feedback in climate change. *Geophysical Research Letters* 36, L09702, doi:10.1029/2009GL038011.

Fletcher,C.G., Zhao, H., Kushner, P.J, Fernandes, R. (2012). Using models and satellite observations to evaluate the strength of snow albedo feedback. *Journal of Geophysical Research*, L09702, doi:10.1029/2009GL038011.

Gordon, H. B. (2002). The CSIRO Mk3 Climate System Model. CSIRO Atmospheric Research Tech. Paper. 60, 134 pp.

Gent, P. R. (2011). The Community Climate System Model Version 4,. *Journal of Climate* , 4973–4991,.

Groisman et al. (2004). Contemporary Changes of the Hydrological Cycle over the Contiguous United States: Trends Derived from In Situ Observations. *Journal of Hydrometeorology*, 5, page 64-84.

Gupta, S. K., W. L. Darnell, and A. C. Wilber, 1992: A parameterization for longwave surface radiation from satellite data: Recent improvements. *Journal of Applied Meteorology of Climatology*, 31, 1361–1367.

Hall, A., Qu, X., Neelin, J.D., 2008. Improving predictions of summer climate change in the United States. *Geophysical Research Letters* 35, L01702, doi:10.1029/2007GL032012.

Hansen, J. G. (1983). Efficient three-dimensional global models for climate studies: Models I and II. Mon. Wea., Rev.,111, 609–662.

Hartmann, D. L. (1994). Global Physical Climatology. San Diego: Academic Press.

Lemke, J. R. (2007). Observations:Changes in Snow, Ice and Frozen Ground. IPCC Fourth Assessment Report, Chapter , page 80-131.

Levis, S., Bonan, G.B., Lawrence, P.J., 2007. Present-day springtime high-latitude surface albedo as a predictor of simulated climate sensitivity. *Geophysical Research Letters* 34, L17703, doi:10.1029/2007GL030775.

Marshall , S.E., 1987. SG WARREN, in: Large Scale Effects of Seasonal Snow Cover: Proceedings of an International Symposium Held During the XIXth General Assembly of the International Union of Geodesy and Geophysics at Vancouver, British Columbia, Canada, 9-22 August 1987. p. 43.

Manabe, W. (1987). Large-Scale Changes of Soil Wetness Induced by an Increase in Atmospheric Carbon Dioxide. : *Journal of The Atmospheric Sciences*, vol. 44, no. 8, pp. 1211-1236, 1987 .

Milly, P.C.D., Shmakin, A.B., 2002. Global modeling of land water and energy balances. Part I: The land dynamics (LaD) model. *Journal of Hydrometeorology* 3, 283–299.

Oke, T.R (1987) Boundary Layer Climates, Second edition, Published in the USA by Methuena and Co. in association with Methuena, Inc. 29 West 35th Street, NY 10001 (p.12).

R. D. Koster, Suarez, M.J., Bounoua, L., Collatz, G.J., Los, S.O., Mahanama, S.P.P., 1996. Influence of the interannual variability of vegetation on the surface energy balance-a global sensitivity study. *Journal of Hydrometeorology* 3, 617–629.

Roeckner, E.A. (1996). The atmospheric general circulation model ECHAM4: Model description and simulation of present-day climate. Max Planck Institute for Meteorology, Rep. 218, 90 pp.

Qu, X., Hall, A., 2006. Assessing snow albedo feedback in simulated climate change. J*ournal of Climate* 19, 2617–2630.

Qu, X., Hall, A., 2007. What Controls the Strength of Snow-Albedo Feedback? *Journal of Climate* 20, 3971–3981.

Solomon, S. D. (2007). Intergovernmental Panel on Climate Change Fourth Assessment Report: Climate Change 2007: Working Group I: The Physical Science Basis. Cambridge, United Kingdom and New York, NY, USA.: Cambridge University Press.

Takata, K., Emori, S., Watanabe, T., 2003. Development of the minimal advanced treatments of surface interaction and runoff. Global and Planetary Change 38, 209–222.

Ting, L. (1993). A diagnostic and modeling study of the monthly mean wintertime anomalies appearing in a 100-year. *Journal of Atmospheric Science*, 50, 2845–2867.

Trenberth, K.E., Fasullo, J.T., Kiehl, J., 2009. Earth's Global Energy Budget. Bulletin of the *American Meteorological Society* 90, 311–323.

Trenberth, K.E., Smith,L. (2005). The Mass of the Atmosphere: A Constraint on Global Analyses. *Journal of Climate*, 18, page 864-875.

Verseghy, D. L. (1993). CLASS—A Canadian land surface scheme for GCMs, II. Vegetation model and coupled runs. *International Journal of Climatology*, 13, 347–370.

Wallace, Z. B. (1996). Interpretation of Interdecadal Trends in Northern Hemisphere Surface Air Temperature. *Journal of Climate*, 9, page 249-259.

Wang, Z., Zeng, X., 2010. Evaluation of Snow Albedo in Land Models for Weather and Climate Studies. *Journal of Applied Meteorology and Climatology* 49, 363–380.

Wetherald, M. (1995). The Mechanisms of Summer Dryness Induced by Greenhouse Warming. *Journal of Climate*,8, page 3096-3108.

Wiscombe, W. (2011, March 3). NASA Earth Observation. Retrieved 01 15, 2012, from Earth Observatory: http://earthobservatory.nasa.gov/Glossary/?mode=all.

Yu, Y. X. (2004). Global coupled ocean atmosphere general circulation models in LASG/IAR Adv. Atmos. Sci., 21, 444–455.